INTERNATIONAL JOURNAL OF
NUMERICAL ANALYSIS AND MODELING
Volume 19, Number 6, Pages 839–863

A PRECONDITIONED STEEPEST DESCENT SOLVER FOR THE CAHN-HILLIARD EQUATION WITH VARIABLE MOBILITY

XIAOCHUN CHEN, CHENG WANG, AND STEVEN M. WISE

Abstract. In this paper we provide a detailed analysis of the preconditioned steepest descent (PSD) iteration solver for a convex splitting numerical scheme to the Cahn-Hilliard equation with variable mobility function. In more details, the convex-concave decomposition is applied to the energy functional, which in turn leads to an implicit treatment for the nonlinear term and the surface diffusion term, combined with an explicit update for the expansive concave term. In addition, the mobility function, which is solution-dependent, is explicitly computed, which ensures the elliptic property of the operator associated with the temporal derivative. The unique solvability of the numerical scheme is derived following the standard convexity analysis, and the energy stability analysis could also be carefully established. On the other hand, an efficient implementation of the numerical scheme turns out to be challenging, due to the coupling of the nonlinear term, the surface diffusion part, and a variable-dependent mobility elliptic operator. Since the implicit parts of the numerical scheme are associated with a strictly convex energy, we propose a preconditioned steepest descent iteration solver for the numerical implementation. Such an iteration solver consists of a computation of the search direction (involved with a Poisson-like equation), and a one-parameter optimization over the search direction, in which the Newton's iteration becomes very powerful. In addition, a theoretical analysis is applied to the PSD iteration solver, and a geometric convergence rate is proved for the iteration. A few numerical examples are presented to demonstrate the robustness and efficiency of the PSD solver.

Key words. Cahn-Hilliard equation, variable mobility function, convex splitting numerical scheme, energy stability, preconditioned steepest descent iteration solver, iteration convergence analysis.

1. Introduction

The Allen-Cahn (AC) [1] (non-conserved dynamics) and Cahn-Hilliard (CH) [4] (conserved dynamics) equations are well known gradient flows with respect to a particular free energy. Suppose that $\Omega \subset \mathbb{R}^d$ (with $d = 2$ or $d = 3$) is a bounded open domain. The CH free energy functional is formulated as

$$E(\phi) = \int_\Omega \left(\frac{1}{4}\phi^4 - \frac{1}{2}\phi^2 + \frac{\varepsilon^2}{2}|\nabla \phi|^2 \right) d\mathbf{x}, \tag{1}$$

for any phase field function $\phi \in H^1(\Omega)$, where ε is an interface width parameter. This free energy is termed *regular* since it is defined for all $\phi \in H^1(\Omega)$. Other free energies, such as those only defined for $0 \le \phi \le 1$, are possible but will not be considered here. For simplicity, we assume that Ω is a rectangular domain, and periodic boundary conditions for ϕ are enforced. The standard CH equation is the conserved gradient flow with respect to the free energy functional (1):

$$\phi_t = \nabla \cdot \Big(\mathcal{M}(\phi) \nabla \mu \Big), \quad \mu := \delta_\phi E = \phi^3 - \phi - \varepsilon^2 \Delta \phi. \tag{2}$$

Received by the editors December 31, 2021 and, in revised form, May 6, 2022; accepted May 23, 2022.

2000 *Mathematics Subject Classification.* 35K30, 65M06, 65M12.

This equation is termed *degenerate* if there are values of ϕ for which $\mathcal{M}(\phi) = 0$. A common choice for the degenerate case is

$$\mathcal{M}(\phi) = \begin{cases} (1+\phi)(1-\phi), & -1 \le \phi \le 1 \\ 0, & |\phi| > 1. \end{cases} \tag{3}$$

Otherwise, the equation is *non-degenerate*. Often times, researchers assume that $\mathcal{M} \equiv 1$, for simplicity. In this paper, we will consider the non-degenerate, non-constant case. In particular, we will assume that, for all ϕ,

$$0 < \mathcal{M}_0 \le \mathcal{M}(\phi) \le \mathcal{M}_1 < \infty. \tag{4}$$

A specific example that we could consider might be the mobility

$$\mathcal{M}(\phi) = \begin{cases} \sqrt{(1+\phi)^2(1-\phi)^2 + \delta^2}, & -1 \le \phi \le 1 \\ \delta, & |\phi| > 1, \end{cases} \tag{5}$$

which is a regularized version of (3). The regularization parameter δ is assumed to be a fixed value, independent on ε. Subsequently, the following energy dissipation law is available, which comes from the gradient structure of (2):

$$\frac{d}{dt} E(\phi(t)) = -\int_\Omega \mathcal{M}(\phi) |\nabla \mu|^2 d\mathbf{x} \le 0. \tag{6}$$

Of course, the usual mass conservative property is valid, i.e., $\int_\Omega \partial_t \phi \, d\mathbf{x} = 0$, which follows from the conservative structure of the equation.

There have been extensive numerical works for the Cahn-Hilliard equation. In particular, energy stability has attracted more and more attentions, since it plays an essential role in the accuracy of long time numerical simulation. The standard convex splitting scheme, pioneered by Eyre's work [16], is a very useful approach to obtain the energy stability at a numerical level. This framework treats the convex part of the chemical potential implicitly and the concave part explicitly. In turn, the unique solvability and energy stability could be theoretically justified by a convexity analysis. An extension to the second order energy stable numerical schemes have also been reported, based on either Crank-Nicolson [12, 15, 24, 25] or BDF-type [10, 43] temporal discretization. Similar ideas have been widely applied to various gradient flows, and both first and second order accurate (in time) algorithms have been developed. See the related works for the phase field crystal (PFC) equation and the modified phase field crystal (MPFC) equation [2, 3, 27, 39, 42]; epitaxial thin film growth models [5, 9, 34, 38]; non-local Cahn-Hilliard-type models [21, 22, 23]; the Cahn-Hilliard-Fluid and related models [6, 7, 13, 14, 20, 26, 41]; *et cetera*. Other than these numerical algorithms, which preserve the energy dissipation in the original phase variable, a few other numerical works have been reported for the reformulated physical system with an introduction of certain auxiliary variables, such as the scalar auxiliary variable (SAV) approach [35, 36, 37]. Some linear numerical schemes with stabilization approach [30, 31, 32, 40] have been reported as well.

Most existing numerical works have been focused on the Cahn-Hilliard flow with a constant mobility function, and the numerical investigation of variable mobility gradient flow turns out to be limited. In addition, the numerical implementation for the variable mobility equation is usually challenging. In this article, we look at a first order accurate in time, energy stable numerical scheme for the Cahn-Hilliard equation, propose a nonlinear iteration solver, and provide a theoretical analysis for the convergence of the solver. For simplicity, we use apply the convex splitting method for the chemical potential, in which the nonlinear term and the surface

diffusion term are treated implicitly, which the expansive concave term is explicitly updated. In addition, the mobility function is computed explicitly, so that the discretization of the temporal derivative corresponds to an elliptic operator. This in turn ensures the unique solvability of the numerical scheme. The energy stability follows from the convex splitting structure of the numerical scheme.

Based on the fact that the numerical method is equivalent to a minimization of a strictly convex energy functional (at the numerical level), we propose the preconditioned steepest descent (PSD) solver for the numerical implementation of the scheme. The PSD solver for the nonlinear p-Laplacian was considered in a pioneering work [28], while an application of the PSD algorithm to a more general, regularized elliptic equation is analyzed in a more recent work [18], in which a much sharper iteration convergence rate has been established if a higher order diffusion term is involved. For the convex splitting numerical scheme applied to the Cahn-Hilliard equation with variable mobility function, the PSD solver turns out to be a very robust tool. The key idea is to use a linearized version of the nonlinear operator as a pre-conditioner to get the search direction. In more details, at each iteration stage, the surface diffusion operator is kept the same as the original form, a constant-coefficient linear operator is used to approximate the nonlinear part in the chemical potential, while a discrete version of $(-\Delta)^{-1}$ is formulated to approximate the temporal derivative, coupled with the variable mobility function. The resulting equation (for the search direction) could be very efficiently solved with the help of FFT, due to the fact that all the linear operators have eigenfunctions exactly same as the Fourier basis functions. Subsequently, once the search direction is obtained, a one-parameter optimization (of the numerical energy functional) over the search direction is taken. In fact, it is a strictly convex optimization in terms of the parameter, the Newton's iteration could be very efficiently implemented. Since the main computation cost at each iteration stage is associated with the Poisson-like solver to obtain the search direction, the numerical implementation of the PSD algorithm is decomposed into the sequence of the Poisson-like solvers.

In addition, we provide a theoretical analysis for the convergence rate of the PSD iteration algorithm, which turns out to be highly challenging, due to the nonlinearity of the numerical scheme, and the variable mobility nature. Fortunately, we are able to recast the equations as equivalent minimization problems involving strictly convex functionals in Hilbert spaces. Because of this fact, the convexity analysis enables us to theoretically derive the convergence analysis for the nonlinear iteration solver. In particular, the non-increasing numerical energy (at each iteration stage) indicates a uniform discrete L^4 bound of the numerical solution in the iteration process, and this nonlinear estimate will play a very important role. Moreover, a careful application of discrete Sobolev embedding makes a connection between the discrete L^4 norm and the corresponding energy norm associated with the precondition stage. All these techniques lead to theoretical justification of the geometric convergence rate for the PSD iteration solver, which is the first result for variable mobility gradient flow equations, to the best of our knowledge.

The rest of this paper is organized as follows. In Section 2, we describe the finite difference discretization of space, recall some basic facts and formulate the first order convex splitting numerical scheme for the variable-mobility Cahn-Hilliard flow. In Section 3, we propose the PSD iteration solver, and provide a theoretical analysis of the geometric convergence rate. Some numerical results are presented in Section 4. Concluding remarks are given in Section 5. For completion, an optimal

rate convergence analysis of the convex-concave numerical approximation scheme for the PDE is provided in Appendix A.

2. Review of the numerical scheme

2.1. The finite difference spatial discretization. The standard centered finite difference spatial approximation is applied. We present the numerical approximation on the computational domain $\Omega = (0,1)^3$ with a periodic boundary condition, and $\Delta x = \Delta y = \Delta z = h = \frac{1}{N}$ with $N \in \mathbb{N}$ to be the spatial mesh resolution throughout this work. In particular, $f_{i,j,k}$ stands for the numerical value of f at the cell centered mesh points $((i+\frac{1}{2})h, (j+\frac{1}{2})h, (k+\frac{1}{2})h)$, and we denote $\mathcal{C}_{\rm per}$ as

$$\mathcal{C}_{\rm per} := \{(f_{i,j,k}) | f_{i,j,k} = f_{i+\alpha N, j+\beta N, k+\gamma N},\ \forall\, i,j,k,\alpha,\beta,\gamma \in \mathbb{Z}\}\,,$$

with the discrete periodic boundary condition imposed. In turn, the discrete average and difference operators are evaluated at $((i+1)h, (j+\frac{1}{2})h, (k+\frac{1}{2})h)$, $((i+\frac{1}{2})h, (j+1)h, (k+\frac{1}{2})h)$ and $((i+\frac{1}{2})h, (j+\frac{1}{2})h, (k+1)h)$, respectively:

$$\begin{aligned}
A_x f_{i+\frac{1}{2},j,k} &:= \frac{1}{2}\left(f_{i+1,j,k} + f_{i,j,k}\right), \quad D_x f_{i+\frac{1}{2},j,k} := \frac{1}{h}\left(f_{i+1,j,k} - f_{i,j,k}\right),\\
A_y f_{i,j+\frac{1}{2},k} &:= \frac{1}{2}\left(f_{i,j+1,k} + f_{i,j,k}\right), \quad D_y f_{i,j+\frac{1}{2},k} := \frac{1}{h}\left(f_{i,j+1,k} - f_{i,j,k}\right),\\
A_z f_{i,j,k+\frac{1}{2}} &:= \frac{1}{2}\left(f_{i,j,k+1} + f_{i,j,k}\right), \quad D_z f_{i,j,k+\frac{1}{2}} := \frac{1}{h}\left(f_{i,j,k+1} - f_{i,j,k}\right).
\end{aligned}$$

Conversely, the corresponding operators at the staggered mesh points are defined as follows:

$$\begin{aligned}
a_x f^x_{i,j,k} &:= \frac{1}{2}\left(f^x_{i+\frac{1}{2},j,k} + f^x_{i-\frac{1}{2},j,k}\right), \quad d_x f^x_{i,j,k} := \frac{1}{h}\left(f^x_{i+\frac{1}{2},j,k} - f^x_{i-\frac{1}{2},j,k}\right),\\
a_y f^y_{i,j,k} &:= \frac{1}{2}\left(f^y_{i,j+\frac{1}{2},k} + f^y_{i,j-\frac{1}{2},k}\right), \quad d_y f^y_{i,j,k} := \frac{1}{h}\left(f^y_{i,j+\frac{1}{2},k} - f^y_{i,j-\frac{1}{2},k}\right),\\
a_z f^z_{i,j,k} &:= \frac{1}{2}\left(f^z_{i,j,k+\frac{1}{2}} + f^z_{i,j,k-\frac{1}{2}}\right), \quad d_z f^z_{i,j,k} := \frac{1}{h}\left(f^z_{i,j,k+\frac{1}{2}} - f^z_{i,j,k-\frac{1}{2}}\right).
\end{aligned}$$

In turn, for a scalar cell-centered function g and a vector function $\vec{f} = (f^x, f^y, f^z)^T$, with f^x, f^y and f^z evaluated at $((i+1)h, (j+\frac{1}{2})h, (k+\frac{1}{2})h)$, $((i+\frac{1}{2})h, (j+1)h, (k+\frac{1}{2})h)$, $((i+\frac{1}{2})h, (j+\frac{1}{2})h, (k+1)h)$, respectively, we define

$$g\vec{f} := \left(A_x g \cdot f^x, A_y g \cdot f^y, A_z g \cdot f^z\right)^T,$$

and the discrete divergence is defined as

$$\nabla_h \cdot \left(g\vec{f}\right)_{i,j,k} = d_x \left(A_x g \cdot f^x\right)_{i,j,k} + d_y \left(A_y g \cdot f^y\right)_{i,j,k} + d_z \left(A_z g \cdot f^z\right)_{i,j,k}. \tag{7}$$

In particular, if $\vec{f} = \nabla_h \phi = (D_x\phi, D_y\phi, D_z\phi)^T$ for a certain scalar grid function ϕ, the corresponding divergence becomes

$$\nabla_h \cdot \left(g \nabla_h \phi\right)_{i,j,k} = d_x \left(A_x g \cdot D_x \phi\right)_{i,j,k} + d_y \left(A_y g \cdot D_y \phi\right)_{i,j,k} + d_z \left(A_z g \cdot D_z \phi\right)_{i,j,k}. \tag{8}$$

Of course, when $g \equiv 1$, have

$$(\Delta_h \phi)_{i,j,k} = \nabla_h \cdot \left(\nabla_h \phi\right)_{i,j,k} = d_x \left(D_x \phi\right)_{i,j,k} + d_y \left(D_y \phi\right)_{i,j,k} + d_z \left(D_z \phi\right)_{i,j,k}. \tag{9}$$

For two cell-centered grid functions f and g, its discrete L^2 inner product and the associated ℓ^2 norm are defined as

$$\langle f, g \rangle := h^3 \sum_{i,j,k=1}^{N} f_{i,j,k} g_{i,j,k}, \quad \|f\|_2 := \left(\langle f, f \rangle\right)^{\frac{1}{2}}.$$

In turn, the mean zero space is introduced as $\mathring{\mathcal{C}}_{\rm per} := \left\{ f \in \mathcal{C}_{\rm per} \;\middle|\; 0 = \overline{f} := \frac{1}{|\Omega|}\langle f, g\rangle \right\}$. Similarly, for two vector grid functions $\vec{f} = (f^x, f^y, f^z)^T$, $\vec{g} = (g^x, g^y, g^z)^T$, with f^x (g^x), f^y (g^y), f^z (g^z) evaluated at $((i+1)h, (j+\frac{1}{2})h, (k+\frac{1}{2})h)$, $((i+\frac{1}{2})h, (j+1)h, (k+\frac{1}{2})h)$, $((i+\frac{1}{2})h, (j+\frac{1}{2})h, (k+1)h)$, respectively, the corresponding discrete inner product is defined as

$$\left[\vec{f}, \vec{g}\right] := [f^x, g^x]_{\rm x} + [g^y, g^y]_{\rm y} + [f^z, g^z]_{\rm z}\,,$$

where

$$[f^x, g^x]_{\rm x} := \langle a_x(f^x g^x), 1\rangle,\;\; [f^y, g^y]_{\rm y} := \langle a_y(f^y g^y), 1\rangle,\;\; [f^z, g^z]_{\rm z} := \langle a_z(f^z g^z), 1\rangle.$$

In addition to the discrete $\|\cdot\|_2$ norm, the discrete maximum norm and ℓ^p norm are defined as

$$\|f\|_p^p := \langle |f|^p, 1\rangle\,,\;\; 1 \le p < \infty, \quad \|f\|_\infty := \max_{1\le i,j,k\le N} |f_{i,j,k}|\,. \tag{10}$$

Moreover, the discrete H_h^1 and H_h^2 norms are introduced as

$$\begin{aligned}
&\|\nabla_h f\|_2^2 := [\nabla_h f, \nabla_h f] = [D_x f, D_x f]_{\rm x} + [D_y f, D_y f]_{\rm y} + [D_z f, D_z f]_{\rm z}\,,\\
&\|f\|_{H_h^1}^2 := \|f\|_2^2 + \|\nabla_h f\|_2^2\,, \quad \|f\|_{H_h^2}^2 := \|f\|_{H_h^1}^2 + \|\Delta_h f\|_2^2.
\end{aligned}$$

The summation by parts formulas are recalled in the following lemma; the detailed proof could be found in [24, 39, 41, 42], *et cetera*.

Lemma 2.1. [24, 39, 41, 42] *For any $\psi, \phi, g \in \mathcal{C}_{\rm per}$, and any $\vec{f} = (f^x, f^y, f_z)^T$, with f^x, f^y, f^z evaluated at $((i+1)h, (j+\frac{1}{2})h, (k+\frac{1}{2})h)$, $((i+\frac{1}{2})h, (j+1)h, (k+\frac{1}{2})h)$, $((i+\frac{1}{2})h, (j+\frac{1}{2})h, (k+1)h)$, respectively, the following summation by parts formulas are valid:*

$$\langle \psi, \nabla_h \cdot \vec{f}\rangle = -\left[\nabla_h \psi, \vec{f}\right], \quad \langle \psi, \nabla_h \cdot (g\nabla_h \phi)\rangle = -\left[\nabla_h \psi, g\nabla_h \phi\right]. \tag{11}$$

In addition, some notation needs to be introduced to facilitate the analysis in later sections. For any $\varphi \in \mathring{\mathcal{C}}_{\rm per}$ and a positive cell centered grid function g (at a point-wise level), the weighed discrete norm is defined as

$$\|\varphi\|_{\mathcal{L}_g^{-1}} = \sqrt{\langle \varphi, \mathcal{L}_g^{-1}(\varphi)\rangle}, \tag{12}$$

where $\psi = \mathcal{L}_g^{-1}(\varphi) \in \mathring{\mathcal{C}}_{\rm per}$ is the unique solution to the discrete Poisson problem

$$\mathcal{L}_g(\psi) := -\nabla_h \cdot (g\nabla_h \psi) = \varphi. \tag{13}$$

In the simplified case of $g \equiv 1$, it is obvious that $\mathcal{L}_g(\psi) = -\Delta_h \psi$, and the discrete H_h^{-1} inner product and H_h^{-1} norm are introduced as $\langle \varphi_1, \varphi_2\rangle_{-1,h} = \langle \varphi_1, (-\Delta_h)^{-1}\varphi_2\rangle$, and $\|\varphi\|_{-1,h} = \sqrt{\langle \varphi, (-\Delta_h)^{-1}\varphi\rangle}$.

2.2. The first order convex splitting numerical scheme. The mobility function at the face-centered mesh points are defined as

$$\begin{aligned}
(\breve{\mathcal{M}}^k)_{i+\frac{1}{2},j,k} &:= A_x(\mathcal{M}(\phi^k))_{i+\frac{1}{2},j,k},\\
(\breve{\mathcal{M}}^k)_{i,j+\frac{1}{2},k} &:= A_y(\mathcal{M}(\phi^k))_{i,j+\frac{1}{2},k},\\
(\breve{\mathcal{M}}^k)_{i,j,k+\frac{1}{2}} &:= A_z(\mathcal{M}(\phi^k))_{i,j,k+\frac{1}{2}}.
\end{aligned} \tag{14}$$

The following finite difference scheme could be applied to the variable-mobility Cahn-Hilliard equation (2): given $\phi^k \in \mathcal{C}_{\rm per}$, find $\phi^{k+1} \in \mathcal{C}_{\rm per}$ such that

$$\frac{\phi^{k+1}-\phi^k}{\Delta t} = \nabla_h \cdot \left(\breve{\mathcal{M}}^k \nabla_h \mu^{k+1} \right), \quad \mu^{k+1} = (\phi^{k+1})^3 - \phi^k - \varepsilon^2 \Delta_h \phi^{k+1}. \tag{15}$$

Regarding the energy stability analysis, the following discrete energy is introduced:

$$E_h(\phi) := \frac{1}{4}\|\phi\|_4^4 - \frac{1}{2}\|\phi\|_2^2 + \frac{\varepsilon^2}{2}\|\nabla_h \phi\|_2^2. \tag{16}$$

The unique solvability and energy stability properties are stated in the following theorem.

Theorem 2.2. *Given $\phi^k \in \mathcal{C}_{\rm per}$, there exists a unique solution $\phi^{k+1} \in \mathcal{C}_{\rm per}$ to the numerical scheme* (15) *with $\phi^{k+1} - \phi^k \in \mathring{\mathcal{C}}_{\rm per}$. In addition, the following energy stability estimate is valid:*

$$E_h(\phi^{k+1}) + \Delta t \left[\breve{\mathcal{M}}^k \nabla_h \mu^{k+1}, \nabla_h \mu^{k+1} \right] \le E_h(\phi^k). \tag{17}$$

Proof. The following nonlinear operator is introduced:

$$\mathcal{N}_h(\phi) := \Big(-\nabla_h \cdot (\breve{\mathcal{M}}^k \nabla_h) \Big)^{-1} (\phi - \phi^k) + \Delta t \phi^3 - \varepsilon^2 \Delta t \Delta_h \phi. \tag{18}$$

The numerical scheme (15) can be expressed equivalently via the following nonlinear system

$$\mathcal{N}_h(\phi) = f := \Delta t \phi^k. \tag{19}$$

Meanwhile, we observed that solving (19) is equivalent to minimizing the following discrete energy functional:

$$J_h(\phi) = \frac{1}{2}\|\phi - \phi^k\|^2_{\mathcal{L}^{-1}_{\breve{\mathcal{M}}^k}} + \frac{\Delta t}{4}\|\phi\|_4^4 + \frac{\varepsilon^2 \Delta t}{2}\|\nabla_h \phi\|_2^2 - \langle f, \phi \rangle, \tag{20}$$

which is defined over the admissible set

$$W_h = \left\{ \phi^{k+1} \in \mathcal{C}_{\rm per} \;\middle|\; \phi^{k+1} - \phi^k \in \mathring{\mathcal{C}}_{\rm per} \right\}.$$

Moreover, J_h is strictly convex in terms of ϕ. As a result, the unique solvability of (19) is a direct consequence of the strict convexity of J_h, following similar arguments as in [42].

The energy stability estimate (17) comes from the convex splitting structure of the numerical scheme. The details are left to interested readers. □

3. The preconditioned steepest descent iteration solver

3.1. The nonlinear iteration solver. The numerical energy functional $J_h(\phi)$ is convex, and its first and second order functional derivatives could be represented in the weak form as

$$\delta_\phi J(\phi)(v) = \left\langle \Big(-\nabla_h \cdot (\breve{\mathcal{M}}^k \nabla_h) \Big)^{-1} (\phi - \phi^k), v \right\rangle + \Delta t \langle \phi^3, v \rangle + \varepsilon^2 \Delta t \langle \nabla_h \phi, \nabla_h v \rangle - \langle f, v \rangle, \tag{21}$$

for any $v \in \mathring{\mathcal{C}}_{\rm per}$, and

$$\delta_\phi^2 J(\phi)(v,w) = \left\langle \Big(-\nabla_h \cdot (\breve{\mathcal{M}}^k \nabla_h) \Big)^{-1} v, w \right\rangle + 3\Delta t \langle \phi^2 v, w \rangle + \varepsilon^2 \Delta t \langle \nabla_h v, \nabla_h w \rangle, \tag{22}$$

for any $v, w \in \mathring{\mathcal{C}}_{\text{per}}$. Applying the discrete Hölder inequality on (21) and (22) yields the following bounds:

(23)
$$|\delta_\phi J(\phi)(v)| \leq \|\phi\|_{\mathcal{L}^{-1}_{\breve{\mathcal{M}}^k}} \|v\|_{\mathcal{L}^{-1}_{\breve{\mathcal{M}}^k}} + \Delta t \|\phi\|_4^3 \|v\|_4 + \varepsilon^2 \Delta t \|\nabla_h \phi\|_2 \|\nabla_h v\|_2 + \|f\|_{4/3} \|v\|_4 ,$$

and

(24)
$$|\delta_\phi^2 J(\phi)(v,w)| \leq \|v\|_{\mathcal{L}^{-1}_{\breve{\mathcal{M}}^k}} \|w\|_{\mathcal{L}^{-1}_{\breve{\mathcal{M}}^k}} + 3\Delta t \|\phi\|_4^2 \|v\|_4 \|w\|_4 + \varepsilon^2 \Delta t \|\nabla_h v\|_2 \|\nabla_h w\|_2 .$$

Again, the discrete numerical energy functional is given by (20). For the discrete $\|\cdot\|_{\mathcal{L}^{-1}_{\breve{\mathcal{M}}^k}}$, the following estimate has been derived in a recent work [33]; the readers are referred for this article for the detailed proof.

Lemma 3.1. [33] *Assume that the mobility function $\mathcal{M}(\phi^k)$ has uniform lower and upper bounds, such that $0 < \mathcal{M}_0 \leq \breve{\mathcal{M}}^k \leq \mathcal{M}_1$. For any $g \in \mathring{\mathcal{C}}_{\text{per}}$, we have*

$$\frac{\mathcal{M}_0}{\mathcal{M}_1^2} \|g\|_{-1,h}^2 \leq \|g\|^2_{\mathcal{L}^{-1}_{\breve{\mathcal{M}}^k}} \leq \frac{\mathcal{M}_1}{\mathcal{M}_0^2} \|g\|_{-1,h}^2. \tag{25}$$

Let us define the operator

$$\mathcal{A}_h \psi := (-\Delta_h)^{-1} \psi + \Delta t \psi - \varepsilon^2 \Delta t \Delta_h \psi, \tag{26}$$

for all $\psi \in \mathring{\mathcal{C}}_{\text{per}}$. This operator is clearly symmetric and positive definite, and it can be efficiently inverted using the FFT. The preconditioned steepest descent method can be formulated as follows: $\phi^{(0)} := \phi^k$, and, for $n \geq 1$,

$$\phi^{(n+1)} = \phi^{(n)} + \alpha_n d_n, \tag{27}$$

where the search direction $d_n \in \mathring{\mathcal{C}}_{\text{per}}$ is defined as the solution to

$$\mathcal{A}_h d_n = f - \mathcal{N}_h(\phi^{(n)}), \tag{28}$$

and the step length α_n is the solution to

$$\alpha_n = \text{argmin}_\alpha J_h(\phi^{(n)} + \alpha d_n) = \text{argzero}_\alpha \left\langle \delta_\phi J_h(\phi^{(n)} + \alpha d_n), d_n \right\rangle . \tag{29}$$

Remark 3.2. *In* (28)*, the computation of $f - \mathcal{N}_h(\phi^{(n)})$ is involves the computation of $\mathcal{L}^{-1}_{\breve{\mathcal{M}}^k}$. In fact, the computation of this inverse operator is equivalent to a minimization of a quadratic energy, so that a preconditioned steepest descent (PSD) solver could be applied. Extensive numerical experiments have implied a computational cost of approximately three Poisson solvers are sufficient to obtain a machine error precision solution for this part. For the optimization problem* (29)*, the Newton's iteration could be applied to obtain an exact solution. Because of the one parameter nature of the optimization, the Newton's iteration turns out to be very efficient. This approach has greatly improved the efficiency of the nonlinear iteration process. Also see* [8, 11, 17, 19, 44] *for the applications of the PSD solver to various gradient flow models.*

3.2. The nonlinear iteration convergence analysis. The following lemma will be used in the later analysis.

Lemma 3.3. *The search direction d_n defined in (28) is the steepest descent direction, at the point $\phi^{(n)} \in W_h$, with respect to the norm $\|\cdot\|_{\mathcal{A}_h}$, where*

$$\|u_n\|^2_{\mathcal{A}_h} = \|u_n\|^2_{-1,h} + \Delta t \|u_n\|_2^2 + \varepsilon^2 \Delta t \|\nabla_h u_n\|_2^2 . \tag{30}$$

Proof. By definition, the (normalized) steepest descent direction at the point $v \in W_h$ is a vector $d \in \mathring{\mathcal{C}}_{\rm per}$ satisfying

$$\delta_\phi J_h(v)(d) = -\left\|\delta_\phi J_h(v)\right\|_{V'}, \quad \|d\|_V = 1, \tag{31}$$

where $\|\cdot\|_V$ is an appropriate norm on $V = \mathring{\mathcal{C}}_{\rm per}$ and $\|\cdot\|_{V'}$ is the standard dual norm defined by

$$\left\|\delta_\phi J_h(v)\right\|_{V'} := \sup_{u\in V=\mathring{\mathcal{C}}_{\rm per}} \frac{|\delta_\phi J_h(v)(u)|}{\|u\|_V}. \tag{32}$$

From (28), the search direction for our scheme satisfies

$$\langle \mathcal{A}_h d_n, v\rangle = -\delta_\phi J_h(\phi^{(n)})(v), \quad \forall\, v \in \mathring{\mathcal{C}}_{\rm per}. \tag{33}$$

Clearly, d_n is the Riesz representation of the functional $-\delta_\phi J_h(\phi^{(n)})$ in the space V with respect to the norm $\|\cdot\|_{\mathcal{A}_h}$. As a consequence,

$$\|d_n\|_{\mathcal{A}_h} = \left\|\delta_\phi J_h(\phi^{(n)})\right\|_{V'}, \tag{34}$$

and

$$\delta_\phi J_h(\phi^{(n)})(d_n) = -\|d_n\|^2_{\mathcal{A}_h} = -\left\|\delta_\phi J_h(\phi^{(n)})\right\|_{V'} \cdot \|d_n\|_{\mathcal{A}_h}, \tag{35}$$

for all $d_n \in V$. □

Corollary 3.4. *Let $\phi^{(n)}$ be the sequence generated by (27), then*

$$J_h(\phi^{(n+1)}) \le J_h(\phi^{(n)}). \tag{36}$$

Lemma 3.5. *Let $\{\phi^{(n)}\}$ be the sequence generated by (27) and $e_n = J_h(\phi^{(n)}) - J_h(\phi)$, where $\phi = \phi^{k+1}$ is the exact solution to* (15)*. Then there exists a constant C_1, independent of ε, such that*

$$\|\phi^{(n)}\|_4 \le C_1, \quad \forall\, n \ge 0. \tag{37}$$

Proof. It follows from the Corollary 3.4 that

$$J_h(\phi^{(n+1)}) \le J_h(\phi^{(n)}) \le \cdots \le J_h(\phi^{(0)}) = \Delta t E_h(\phi^k) \le \cdots \le \Delta t E_h(\phi^0) \le \Delta t C_0, \tag{38}$$

where $C_0 > 0$ is independent of $h > 0$. Since

$$J_h(\phi) = \frac{1}{2}\left\|\phi - \phi^k\right\|^2_{\mathcal{L}^{-1}_{\mathcal{M}^k}} + \frac{\Delta t}{4}\|\phi\|_4^4 + \frac{\varepsilon^2\Delta t}{2}\|\nabla_h\phi\|_2^2 - \Delta t(\phi^k, \phi), \tag{39}$$

it follows that

$$\begin{aligned} J_h(\phi^{(n)}) &\ge \frac{\Delta t}{4}\left\|\phi^{(n)}\right\|_4^4 + \frac{\varepsilon^2\Delta t}{2}\left\|\nabla_h\phi^{(n)}\right\|_2^2 - \Delta t(\phi^k, \phi^{(n)}) \\ &\ge \frac{\Delta t}{4}\left\|\phi^{(n)}\right\|_4^4 + \frac{\varepsilon^2\Delta t}{2}\left\|\nabla_h\phi^{(n)}\right\|_2^2 - \frac{\Delta t}{2}(\|\phi^k\|_2^2 + \|\phi^{(n)}\|_2^2), \end{aligned}$$

so that

$$\begin{aligned} \frac{\Delta t}{4}\left\|\phi^{(n)}\right\|_4^4 + \frac{\varepsilon^2\Delta t}{2}\left\|\nabla_h\phi^{(n)}\right\|_2^2 - \frac{\Delta t}{2}\|\phi^{(n)}\|_2^2 &\le \Delta t E_h(\phi^k) + \frac{\Delta t}{2}\|\phi^k\|_2^2 \\ &\le \Delta t C_0 + \frac{\Delta t}{2}\|\phi^k\|_2^2. \end{aligned} \tag{40}$$

Meanwhile, taking a look at the detailed form of $E_h(\phi^k)$, we observe that

$$\begin{aligned} C_0 &\geq E_h(\phi^k) \\ &= \frac{1}{4}\|\phi^k\|_4^4 - \frac{1}{2}\|\phi^k\|_2^2 + \frac{\varepsilon^2}{2}\|\nabla_h\phi^k\|_2^2 \\ &\geq \frac{1}{8}\|\phi^k\|_4^4 - \frac{1}{2}|\Omega| + \frac{\varepsilon^2}{2}\|\nabla_h\phi^k\|_2^2, \end{aligned} \tag{41}$$

where we have used the following quadratic inequality:

$$\frac{1}{8}x^4 - \frac{1}{2}x^2 \geq -\frac{1}{2}, \quad \forall\, x \in \mathbb{R}. \tag{42}$$

Then we get

$$\|\phi^k\|_4 \leq \left(8C_0 + 4|\Omega|\right)^{1/4}. \tag{43}$$

Furthermore, with an application of discrete Hölder inequality, we arrive at

$$\|\phi^k\|_2 \leq \|\phi^k\|_4 \cdot |\Omega|^{1/4} \leq \left(8C_0|\Omega| + 4|\Omega|^2\right)^{1/4}. \tag{44}$$

Going back to (40), we get

$$\frac{1}{4}\|\phi^{(n)}\|_4^4 + \frac{\varepsilon^2}{2}\|\nabla_h\phi^{(n)}\|_2^2 - \frac{1}{2}\|\phi^{(n)}\|_2^2 \leq C_0 + \frac{1}{2}\left(8C_0|\Omega| + 4|\Omega|^2\right)^{1/2}. \tag{45}$$

Again, we apply a quadratic inequality and observe that

$$\frac{1}{8}\|\phi^{(n)}\|_4^4 - \frac{1}{2}\|\phi^{(n)}\|_2^2 \geq -\frac{1}{2}|\Omega|. \tag{46}$$

Substitution of the last inequality into (45) yields

$$\frac{1}{8}\|\phi^{(n)}\|_4^4 + \frac{\varepsilon^2}{2}\|\nabla_h\phi^{(n)}\|_2^2 \leq C_0 + \frac{1}{2}\left(8C_0|\Omega| + 4|\Omega|^2\right)^{1/2} + \frac{1}{2}|\Omega|. \tag{47}$$

Therefore, we have

$$\|\phi^{(n)}\|_4 \leq \left(8C_0 + 4(8C_0|\Omega| + 4|\Omega|^2)^{1/2} + 4|\Omega|\right)^{1/4} =: C_1, \tag{48}$$

as desired. In a similar fashion, we also get

$$\|\nabla_h\phi^{(n)}\|_2 \leq \varepsilon^{-1}\left(2C_0 + (8C_0|\Omega| + 4|\Omega|^2)^{1/2} + |\Omega|\right)^{1/2}. \tag{49}$$

Note that constant C_1 is ε-independent. This completes the proof of Lemma 3.5. □

The following lemma gives a discrete 2-D Sobolev inequality, from H^1 into L^4; the detailed proof could be found in an existing work [18].

Proposition 3.6. [18] *For all $\phi \in \mathring{\mathcal{C}}_{\rm per}$, we have*

$$\|\phi\|_4 \leq B_0\, \|\phi\|_{-1,h}^{\frac{1}{4}} \cdot \|\nabla_h\phi\|_2^{\frac{3}{4}}, \tag{50}$$

for some constant $B_0 > 0$ that depends only upon Ω.

The following inequality plays an important role in the nonlinear iteration analysis.

Lemma 3.7. *For any $u, v \in \mathring{\mathcal{C}}_{\rm per}$, the following inequality is valid:*

$$\langle \delta_\phi J_h(u) - \delta_\phi J_h(v), u - v\rangle \geq C_2\, \|u - v\|_{\mathcal{A}_h}^2, \tag{51}$$

where

$$C_2 := \min\left(\frac{\mathcal{M}_0}{2\mathcal{M}_1^2}, \frac{1}{2}, \frac{\mathcal{M}_0^{\frac{1}{2}}\varepsilon}{\mathcal{M}_1}\Delta t^{-\frac{1}{2}}\right).$$

Proof. A careful calculation reveals that

$$\langle \delta_\phi J_h(u) - \delta_\phi J_h(v), u - v\rangle = \|u-v\|^2_{\mathcal{L}^{-1}_{\breve{\mathcal{M}}^k}} + \varepsilon^2 \Delta t \|\nabla_h (u-v)\|_2^2 + \Delta t \langle u^3 - v^3, u - v\rangle. \tag{52}$$

Meanwhile, the following estimate is available:

$$\langle u^3 - v^3, u - v\rangle \geq 0. \tag{53}$$

As a consequence, we get

$$\begin{aligned} \langle \delta_\phi J_h(u) - \delta_\phi J_h(v), u - v\rangle &\geq \|u-v\|^2_{\mathcal{L}^{-1}_{\breve{\mathcal{M}}^k}} + \varepsilon^2 \Delta t \|\nabla_h (u-v)\|_2^2 \\ &\geq \frac{\mathcal{M}_0}{\mathcal{M}_1^2} \|u-v\|^2_{-1,h} + \varepsilon^2 \Delta t \|\nabla_h (u-v)\|_2^2 \\ &\geq \frac{\mathcal{M}_0}{2\mathcal{M}_1^2} \|u-v\|^2_{-1,h} + \frac{1}{2}\varepsilon^2 \Delta t \|\nabla_h (u-v)\|_2^2 \\ &\quad + \frac{\mathcal{M}_0^{\frac{1}{2}}\varepsilon}{\mathcal{M}_1} \sqrt{\Delta t} \|u-v\|_2^2, \end{aligned} \tag{54}$$

in which the second step comes from inequality (25) (in Lemma 3.1), and the third step is the direct consequence of the following Cauchy inequality:

$$\begin{aligned} \frac{\mathcal{M}_0}{2\mathcal{M}_1^2} \|u-v\|^2_{-1,h} + \frac{1}{2}\varepsilon^2 \Delta t \|\nabla_h (u-v)\|_2^2 &\geq \frac{\mathcal{M}_0^{\frac{1}{2}}\varepsilon}{\mathcal{M}_1} \sqrt{\Delta t} \|u-v\|_{-1,h} \cdot \|\nabla_h (u-v)\|_2 \\ &\geq \frac{\mathcal{M}_0^{\frac{1}{2}}\varepsilon}{\mathcal{M}_1} \sqrt{\Delta t} \|u-v\|_2^2. \end{aligned} \tag{55}$$

Finally, considering

$$\|u-v\|^2_{\mathcal{A}_h} = \|u-v\|^2_{-1,h} + \Delta t \|\nabla_h (u-v)\|_2^2 + \varepsilon^2 \Delta t \|\nabla_h (u-v)\|_2^2, \tag{56}$$

we conclude that estimate (51) is valid by choosing C_2 as indicated above. □

Lemma 3.8. *The iteration error is defined as $e_n := J_h(\phi^{(n)}) - J_h(\phi)$. With the same assumptions as Lemma 3.5, we have*

$$e_n \leq \langle \delta_\phi J_h(\phi^{(n)}) - \delta_\phi J_h(\phi), \phi^{(n)} - \phi\rangle \leq C_3 \left\| \delta_\phi J_h(\phi^{(n)}) \right\|^2_{V'}, \tag{57}$$

and

$$\left| \delta_\phi^2 J_h(\theta^n)(d_n, d_n) \right| \leq C_4 \|d_n\|^2_{\mathcal{A}_h}, \tag{58}$$

for any θ^n in the line segment from $\phi^{(n)}$ to $\phi^{(n+1)}$, where the constants $C_3, C_4 >$ take the following forms:

$$\begin{aligned} C_3 &:= C_2^{-1} = \max\Big(2, \frac{2\mathcal{M}_1^2}{\mathcal{M}_0}, \frac{\mathcal{M}_1}{\mathcal{M}_0^{\frac{1}{2}}\varepsilon} \Delta t^{\frac{1}{2}}\Big), \\ C_4 &:= \max(1, \mathcal{M}_1 \mathcal{M}_0^{-2}) + \frac{1}{4} \cdot 3^{\frac{7}{4}} B_0^2 C_1^2 \varepsilon^{-\frac{3}{2}} \Delta t^{\frac{1}{4}}, \end{aligned} \tag{59}$$

with C_1, B_0 as given in Lemmas 3.5, 3.6, respectively.

Proof. By convexity of J_h, we have

$$J_h(\phi^{(n)}) - J_h(\phi) \leq \langle \delta_\phi J_h(\phi^{(n)}) - \delta_\phi J_h(\phi), \phi^{(n)} - \phi\rangle. \tag{60}$$

With an application of inequality (51) in Lemma 3.7, we arrive at

$$\begin{aligned}\langle \delta_\phi J_h(\phi^{(n)}) - \delta_\phi J_h(\phi), \phi^{(n)} - \phi\rangle &= \langle \delta_\phi J_h(\phi^{(n)}), \phi^{(n)} - \phi\rangle \\ &\leq \left\|\delta_\phi J_h(\phi^{(n)})\right\|_{V'} \left\|\phi - \phi^{(n)}\right\|_{\mathcal{A}_h} \\ &\leq \frac{1}{2}C_2^{-1}\left\|\delta_\phi J_h(\phi^{(n)})\right\|_{V'}^2 + \frac{1}{2}C_2\left\|\phi - \phi^{(n)}\right\|_{\mathcal{A}_h}^2 \\ &\leq \frac{1}{2}C_2^{-1}\left\|\delta_\phi J_h(\phi^{(n)})\right\|_{V'}^2 + \frac{1}{2} \\ &\quad \langle \delta_\phi J_h(\phi^{(n)}) - \delta_\phi J_h(\phi), \phi^{(n)} - \phi\rangle.\end{aligned} \tag{61}$$

Therefore, we can take constant $C_3 = C_2^{-1} = \max(2, \Delta t^{\frac{1}{2}}\epsilon^{-1})$, such that

$$e^n \leq \langle \delta_\phi J_h(\phi^{(n)}) - \delta_\phi J_h(\phi), \phi^{(n)} - \phi\rangle \leq C_3\left\|\delta_\phi J_h(\phi^{(n)})\right\|_{V'}^2. \tag{62}$$

Next we derive a bound for $\left|\delta_\phi^2 J_h(\theta^n)(d_n, d_n)\right|$. We begin with an application of (24):

$$\left|\delta_\phi^2 J_h(\theta^n)(d_n, d_n)\right| \leq \|d_n\|_{\mathcal{L}^{-1}_{\breve{\mathcal{M}}^k}}^2 + 3\Delta t\,\|\theta^n\|_4^2 \cdot \|d_n\|_4^2 + \varepsilon^2\Delta t\,\|\nabla_h d_n\|_2^2. \tag{63}$$

With the help of the ℓ^4 estimate (37) (in Lemma 3.5), we get

$$\|\theta^n\|_4 \leq C_1. \tag{64}$$

On the other hand, an application of discrete Sobolev inequality (50) (in Proposition 3.6) indicates that

$$\begin{aligned}\|d_n\|_{-1,h}^2 + \varepsilon^2\Delta t\,\|\nabla_h d_n\|_2^2 &\geq \frac{4}{3^{3/4}}\varepsilon^{\frac{3}{2}}\Delta t^{\frac{3}{4}}\,\|d_n\|_{-1,h}^{\frac{1}{2}} \cdot \|\nabla_h d_n\|_2^{\frac{3}{2}} \\ &\geq \frac{4}{3^{3/4}}\varepsilon^{\frac{3}{2}}\Delta t^{\frac{3}{4}}B_0^{-2}\,\|d_n\|_4^2,\end{aligned} \tag{65}$$

with the Young's inequality applied in the first step. Consequently, a substitution of (64) and (65) into (63) yields

$$\begin{aligned}\left|\delta_\phi^2 J_h(\theta^n)(d_n, d_n)\right| &\leq \frac{\mathcal{M}_1}{\mathcal{M}_0^2}\,\|d_n\|_{-1,h}^2 + \varepsilon^2\Delta t\,\|\nabla_h d_n\|_2^2 + 3\Delta t\,\|\theta^n\|_4^2 \cdot \|d_n\|_4^2 \\ &\leq \left(\max(1, \mathcal{M}_1\mathcal{M}_0^{-2}) + \frac{1}{4}\cdot 3^{\frac{7}{4}}B_0^2C_1^2\epsilon^{-\frac{3}{2}}\Delta t^{\frac{1}{4}}\right)(\|d_n\|_{-1,h}^2 + \varepsilon^2 s\,\|\nabla_h d_n\|_2^2),\end{aligned} \tag{66}$$

Considering

$$\|d_n\|_{\mathcal{A}_h}^2 = \|d_n\|_{-1,h}^2 + \Delta t\,\|d_n\|_2^2 + \varepsilon^2\Delta t\,\|\nabla_h d_n\|_2^2, \tag{67}$$

we conclude that estimate (58) is valid by choosing $C_4 = \max(1, \mathcal{M}_1\mathcal{M}_0^{-2}) + \frac{1}{4}\cdot 3^{\frac{7}{4}}B_0^2C_1^2\epsilon^{-\frac{3}{2}}\Delta t^{\frac{1}{4}}$. Note that both B_0 and C_1 are ε, Δt independent. This finishes the proof of Lemma 3.8. □

Remark 3.9. *We see that $C_3 = O(1)$ if $\Delta t = O(\varepsilon^2)$, while $C_3 = O(\varepsilon^{-1}\Delta t^{\frac{1}{2}})$ with a small ε value. A similar scaling law is available for C_4: $C_4 = O(\varepsilon^{-1})$ if $\Delta t = O(\varepsilon^2)$, while $C_4 = O(\varepsilon^{-\frac{3}{2}}\Delta t^{\frac{1}{4}})$ with a small ε value.*

For the case of $d = 3$, $p = 4$, the discrete Sobolev inequality becomes

$$\|\phi\|_4 \leq B_0\|\phi\|_{-1,h}^{\frac{1}{8}} \cdot \|\nabla_h\phi\|_2^{\frac{7}{8}}, \quad \forall\,\phi \in \mathring{\mathcal{C}}_{\mathrm{per}}. \tag{68}$$

The estimates corresponding to (63)-(65) turn out to be

$$\left|\delta_\phi^2 J_h(\theta^n)(d_n, d_n)\right| \leq \|d_n\|_{\mathcal{L}^{-1}_{\breve{\mathcal{M}}^k}}^2 + 3\Delta t\,\|\theta^n\|_4^2\,\|d_n\|_4^2 + \varepsilon^2\Delta t\,\|\nabla_h d_n\|_2^2, \tag{69}$$

$$\|\theta^n\|_4 \le C_1, \tag{70}$$

and

$$\|d_n\|_{-1,h}^2+\varepsilon^2\Delta t\,\|\nabla_h d_n\|_2^2 \ge \frac{8}{7^{7/8}}\varepsilon^{\frac{7}{4}}\Delta t^{\frac{7}{8}}\,\|d_n\|_{-1,h}^{\frac{1}{4}}\cdot\|\nabla_h d_n\|_2^{\frac{7}{4}} \ge \frac{8}{7^{7/8}}\varepsilon^{\frac{7}{4}}\Delta t^{\frac{7}{8}}B_0^{-2}\,\|d_n\|_4^2\,. \tag{71}$$

Then we get

$$\begin{aligned}&\left|\delta_\phi^2 J_h(\theta^n)(d_n,d_n)\right|\\ \le&\Big(\max(1,\mathcal{M}_1\mathcal{M}_0^{-2})+\frac{3}{8}\cdot 7^{7/8}\varepsilon^{-\frac{7}{4}}\Delta t^{\frac{1}{4}}C_1^2B_0^2\Big)\,(\|d_n\|_2^2+\epsilon^2 s\,\|\Delta_h d_n\|_2^2).\end{aligned} \tag{72}$$

In comparison with (67), we conclude that estimate (58) is valid by choosing

$$C_4=\max(1,\mathcal{M}_1\mathcal{M}_0^{-2})+\frac{3}{8}\cdot 7^{7/8}\varepsilon^{-\frac{7}{4}}\Delta t^{\frac{1}{4}}C_1^2B_0^2.$$

Theorem 3.10. *Let $\{\phi^{(n)}\}$ be the sequence generated by (27). Then*

$$e_n\le C_5^n e_0,\quad \textit{where}\quad C_5:=1-\frac{1}{2C_3C_4}. \tag{73}$$

Proof. For any α from the definition of the steepest descent direction, we apply (58) from Lemma 3.8 and get

$$\begin{aligned}J_h(\phi^{(n)}+\alpha d_n)-J_h(\phi^{(n)}) &= \alpha\delta_\phi J_h(\phi^{(n)})(d_n)+\frac{\alpha^2}{2}\delta_\phi^2 J_h(\theta)(d_n,d_n)\\ &\le \alpha\delta_\phi J_h(\phi^{(n)})(d_n)+\frac{\alpha^2}{2}C_4\,\|d_n\|_{\mathcal{A}_h}^2\\ &= \big(-\alpha+\frac{\alpha^2}{2}C_4\big)\left\|\delta_\phi J_h(\phi^{(n)})\right\|_{V'}^2.\end{aligned} \tag{74}$$

Hence the minimum achieved at $\alpha_n=\frac{1}{C_4}$. Then we have

$$\begin{aligned}e_{n+1}-e_n &= J_h(\phi^{(n+1)})-J_h(\phi^{(n)})\\ &\le J_h(\phi^{(n)}+\alpha_n d_n)-J_h(\phi^{(n)})\\ &= -\frac{1}{2C_4}\left\|\delta_\phi J_h(\phi^{(n)})\right\|_{V'}^2.\end{aligned} \tag{75}$$

Therefore,

$$\begin{aligned}e_n-e_{n+1} &\ge \frac{1}{2C_4}\left\|\delta_\phi J_h(\phi^{(n)})\right\|_{V'}^2\\ &\ge \frac{1}{2C_3C_4}e_n,\end{aligned} \tag{76}$$

in which the estimate (57) of Lemma 3.8 was applied in the last step. Hence,

$$e_{n+1}\le\left(1-\frac{1}{2C_3C_4}\right)e_n. \tag{77}$$

Then the desired result follows. □

In fact, by the representation formula (59), we see that $C_3\ge 2$, $C_4\ge 1$, so that $0<C_5=1-\frac{1}{2C_3C_4}<1$.

Remark 3.11. *A geometric convergence rate is assured by Theorem 3.10. Regarding the convergence constant, we observe that $C_3C_4=O(\varepsilon^{-1})$ for a time step choice $\Delta t=O(\varepsilon^2)$, while $C_3C_4=O(\varepsilon^{-\frac{5}{2}}\Delta t^{\frac{3}{4}})$ with a small ε value. In turn, this*

estimate leads to a convergence rate of α_0^n*, with* $0 < \alpha_0 < 1$ *for* $\Delta t = O(\varepsilon^2)$*, while* $\alpha_0 = 1 - O(\Delta t^{-\frac{3}{4}} \varepsilon^{\frac{5}{2}})$ *in a general numerical set-up.*

This analysis also verifies the following well-known fact observed in the extensive numerical experiments: the steepest descent nonlinear iteration provides a fast convergence for a small time step size. With a smaller value of ε*, the numerical implementation becomes more and more challenging. Moreover, a small time step size also accelerates the convergence speed for a small value of* ε*.*

The contraction estimate (77) is valid for the error of the discrete energy (20). Meanwhile, such a contraction estimate is not directly available for the numerical error of the original phase variable: $q_n := \phi^{(n)} - \phi$. However, we are still able to derive a geometric convergent estimate for such a numerical error. The functional inequality is available

$$\begin{aligned} J_h(\phi^{(n)}) - J_h(\phi) &= \delta_\phi J_h(\phi)(q_n) + \frac{1}{2}\delta_\phi^2 J_h(\theta)(q_n, q_n) \\ &= \frac{1}{2}\delta_\phi^2 J_h(\theta)(q_n, q_n) \\ &\geq \frac{\mathcal{M}_0}{2\mathcal{M}_1^2}\|q_n\|_{-1,h}^2 + \frac{\varepsilon^2 \Delta t}{2}\|\nabla_h q_n\|_2^2, \end{aligned} \tag{78}$$

with θ in the line segment from $\phi^{(n)}$ to ϕ. Note that the second step comes from the fact that $\delta_\phi J_h(\phi) \equiv 0$, and the following fact is used in the last step:

$$3\theta^2 (q_n)^2 \geq 0. \tag{79}$$

As a direct consequence, we get

$$\begin{aligned} \frac{\mathcal{M}_0}{2\mathcal{M}_1^2}\|q_n\|_{-1,h}^2 + \frac{\varepsilon^2 \Delta t}{2}\|\nabla_h q_n\|_2^2 \leq & e_n \\ \leq & C_5^n e_0 \\ \leq & (C_5)^n \Big(-\frac{1}{2}\|\phi - \phi^k\|_{\mathcal{L}_{\breve{\mathcal{M}}^k}^{-1}}^2 + \frac{\Delta t}{4}(\|\phi^k\|_4^4 - \|\phi\|_4^4) \\ & + \frac{\varepsilon^2 \Delta t}{2}(\|\nabla_h \phi^k\|_2^2 - \|\nabla_h \phi\|_2^2) + \Delta t(\phi^k, \phi^k - \phi)\Big) \\ \leq & \Delta t (C_5)^n R_k, \end{aligned} \tag{80}$$

where

$$R_k = \frac{1}{4}(\|\phi^k\|_4^4 - \|\phi\|_4^4) + \frac{\varepsilon^2}{2}(\|\nabla_h \phi^k\|_2^2 - \|\nabla_h \phi\|_2^2) + (\phi^k, \phi^k - \phi).$$

This yields the geometric convergence analysis for the numerical error q_n, in both $\|\cdot\|_2$ and discrete H_h^1 norms. We also notice that $R_k = O(\Delta t)$, since ϕ is the exact numerical solution ϕ^{k+1} for the convex splitting scheme.

4. Numerical results

4.1. Convergence test for the numerical schemes. In this subsection we perform a numerical accuracy check for the numerical scheme (15). The computational domain is chosen as $\Omega = (0, 1)^2$, and the exact profile for the phase variable is set to be

$$\Phi(x, y, t) = \frac{1}{\pi}\sin(2\pi x)\cos(2\pi y)\cos(t). \tag{81}$$

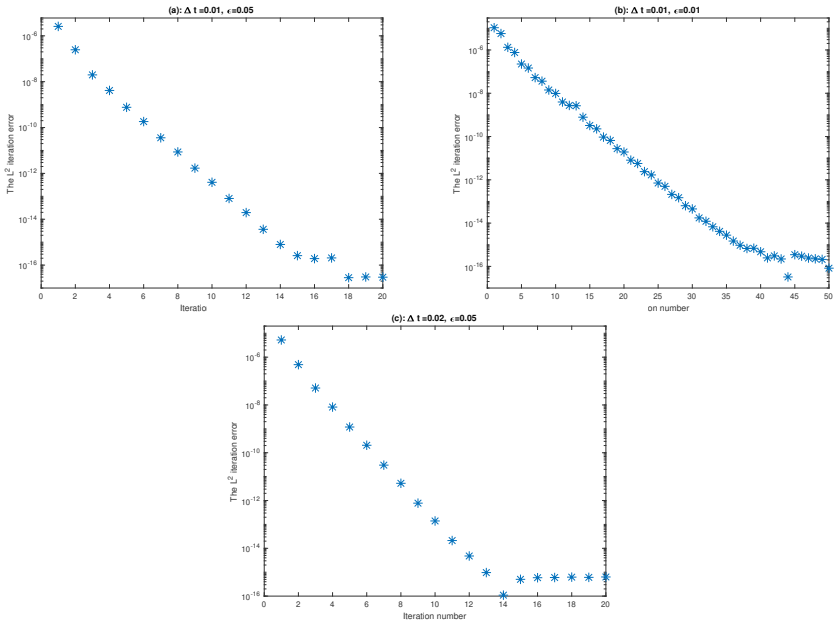

FIGURE 1. The discrete ℓ^2 numerical errors vs. the iteration number, with a spatial resolution $N = 256$. The numerical results are obtained by the proposed PSD iteration solver. The time step size and surface diffusion parameters are taken as: (a) $\Delta t = 0.01$, $\varepsilon = 0.05$, (b) $\Delta t = 0.01$, $\varepsilon = 0.01$, and (c) $\Delta t = 0.02$, $\varepsilon = 0.05$.

To make Φ satisfy the original PDE (2), we have to add an artificial, time-dependent forcing term. Then the numerical scheme (15) can be implemented to solve for (2). In addition, we set the mobility function as

$$\mathcal{M}(\phi) = \frac{1}{2}(1 + \phi^2). \tag{82}$$

Notice that this mobility function has a uniform lower bound $\mathcal{M}(\phi) \geq \frac{1}{2}$.

First, we verify the efficiency and accuracy of the proposed PSD iterative solver. The first time step is taken into consideration, and we take the spatial resolution as $N = 256$ (with $h = \frac{1}{256}$). To investigate the iteration performance and its dependence on certain parameters, such as the time step size Δt and interface width ε, we take three different parameter combinations: (a) $\Delta t = 0.01$, $\varepsilon = 0.05$, (b) $\Delta t = 0.01$, $\varepsilon = 0.01$, and (c) $\Delta t = 0.02$, $\varepsilon = 0.05$. The discrete ℓ^2 iteration errors are displayed in Figure 1, in terms of the iteration number.

In all three cases, the geometric convergence rate has been clearly observed in the iteration process, which justifies the theoretical analysis (80). In addition, the convergence rate turns out to be faster with a smaller time step size Δt or a larger surface diffusion parameter ε, by making a comparison between (a) and (b), (a) and (c), respectively. This numerical behavior also agrees with the analysis outlined in Remark 3.11. Meanwhile, all these iterations have reached the machine precision within 40 iteration stages. In the practical computations, only 5 to 10 iteration stages are needed at each time step.

Next, the accuracy check for the fully implemented numerical scheme is performed. The spatial resolution is fixed as $N = 256$ so that the spatial numerical

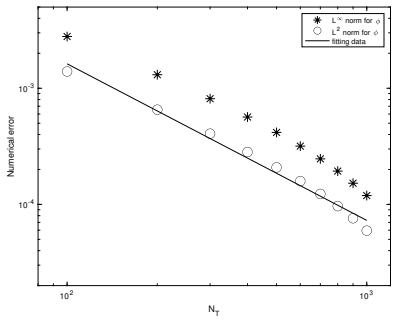

FIGURE 2. The discrete ℓ^2 and ℓ^∞ numerical errors versus temporal resolution N_T for $N_T = 100 : 100 : 1000$, with a spatial resolution $N = 256$. The numerical results are obtained by the computation using the numerical scheme (15). The surface diffusion parameter is taken to be $\varepsilon = 0.5$. The data lie roughly on curves $CN_T^{-a_e}$ for appropriate choices of C, with $a_e = 1.3463$, confirming the first order temporal accuracy of the scheme.

error is negligible. The final time is set as $T = 1$, and the surface diffusion parameter is taken as $\varepsilon = 0.5$. Naturally, a sequence of time step sizes are taken as $\Delta t = \frac{T}{N_T}$ with $N_T = 100 : 100 : 1000$. The expected temporal numerical accuracy assumption $e = C\Delta t$ indicates that $\ln|e| = \ln(CT) - \ln N_T$, so that we plot $\ln|e|$ versus. $\ln N_T$ to demonstrate the temporal convergence order. The fitted line displayed in Figure 2 shows an approximate slope of -1.3463, which in turn verifies at least first order temporal convergence order in both the discrete ℓ^2 and ℓ^∞ norms.

4.2. Numerical simulation of coarsening processes. In this subsection, we perform a two-dimensional numerical simulation showing the coarsening process with variable mobility function (82). The computational domain is set as $\Omega = (0,1)^2$, and the interface width parameter is taken as $\varepsilon = 0.005$. The initial data are given by

(83)
$$\phi_{i,j}^0 = 0.05 \cdot (2r_{i,j} - 1), \quad r_{i,j} \text{ are uniformly distributed random numbers in } [0,1].$$

The numerical scheme (15) is implemented for this simulation. For the temporal step size Δt, we use increasing values of Δt in the time evolution: $\Delta t = 5 \times 10^{-5}$ on the time interval $[0, 0.5]$, $\Delta t = 10^{-4}$ on the time interval $[0.5, 3]$ and $\Delta t = 2 \times 10^{-4}$ on the time interval $[3, 7]$. Whenever a new time step size is applied, we initiate the two-step numerical scheme by taking $\phi^{-1} = \phi^0$, with the initial data ϕ^0 given by the final time output of the last time period. The time snapshots of the evolution by using $\varepsilon = 0.005$ are presented in Figure 3, with significant coarsening observed in the system. At early times many small structures are present. At the final time, $t = 7$, a single structure emerges, and further coarsening is not possible.

In particular, the long time characteristics of the solution, especially the energy decay rate, are of great scientific interests. For the epitaxial thin film growth and polynomial-approximation Cahn-Hilliard gradient models, certain theoretical analysis [29] has provided an upper bound of the energy decay rate as $t^{-1/3}$, and some numerical experiments have also demonstrated such a scaling law [10, 12]. Meanwhile, for the Cahn-Hilliard flow with variable mobility function, the energy dissipation law has also been an interesting issue. In this article, we provide some

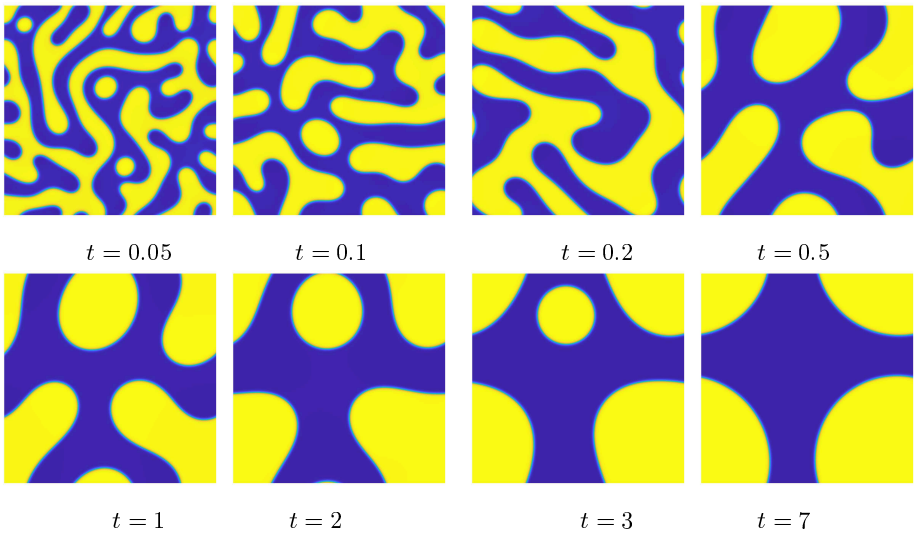

FIGURE 3. (Color online.) Snapshots of the phase variable ϕ at the indicated time instants over the domain $\Omega = (0,1)^2$, $\varepsilon = 0.005$, with the solution-dependent mobility (82). Finally, there is a single structure at $t = 7$.

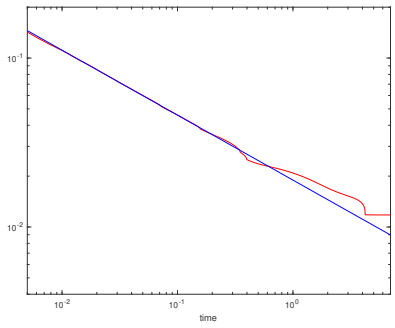

FIGURE 4. Log-log plot of the temporal evolution the energy E_h for $\varepsilon = 0.005$, with a variable mobility function given by (82). The energy decreases like $a_e t^{b_e}$ until saturation. The red lines represent the energy plot obtained by the simulations, while the straight lines are obtained by least squares approximations to the energy data. The least squares fit is only taken for the linear part of the calculated data, only up to about time $t = 100$. The fitted line has the form $a_e t^{b_e}$, with $a_e = 0.01895$, $b_e = -0.3845$.

numerical evidences. Figure 4 presents the log-log plot for the energy versus time, with the given physical parameters, in which the discrete E_h is defined as (16). The detailed scaling "exponent" is obtained using least squares fits of the computed data up to time $t = 100$. A clear observation of the $a_e t^{b_e}$ scaling law can be made, with $a_e = 0.01895$, $b_e = -0.3845$. It is amazing to obtain an energy dissipation scaling index for the Flory-Huggins Cahn-Hilliard flow in the long time

numerical simulation, which is close to the $t^{-1/3}$ scaling observed in the polynomial approximation model.

5. Concluding remarks

In this article, the preconditioned steepest descent (PSD) iteration solver is considered to implement a first order convex splitting numerical scheme, combined with the finite difference spatial discretization, to the Cahn-Hilliard equation with variable mobility function. The convex-concave decomposition is applied to the energy functional, while the mobility function is explicitly updated to ensure the unique solvability. In terms of the numerical implementation of this nonlinear numerical scheme, coupled with a variable-mobility approximation, we propose a preconditioned steepest descent iteration solver in the computation, since the implicit parts of the numerical scheme are associated with a strictly convex energy. Such an iteration solver consists of a computation of the search direction (involved with a Poisson-like equation), and a one-parameter optimization over the search direction, in which the Newton's iteration becomes very powerful. At a theoretical level, a geometric convergence rate is proved for the PSD iteration, which is the first such result for the variable-mobility gradient flows. In addition, an optimal rate convergence analysis and error estimate have also been established for the fully discrete finite difference scheme. A few numerical examples are presented to demonstrate the robustness and efficiency of the PSD solver.

Acknowledgements

This work is supported in part by the National Science Foundation (USA) grants NSF DMS-2012269 (C. Wang), and NSF DMS-1719854, DMS-2012634 (S. Wise).

Appendix A. The convergence analysis for the numerical scheme

In this appendix we provide an optimal rate convergence analysis for the fully discrete scheme (15). Let Φ be the exact PDE solution for the variable-mobility Cahn-Hillaird equation (2). With sufficiently regular initial data, it is reasonable to assume that the exact solution has regularity of class $\mathcal{R}$, where

$$\Phi \in \mathcal{R} := H^2\left(0,T;C_{\rm per}(\Omega)\right) \cap H^1\left(0,T;C^2_{\rm per}(\Omega)\right) \cap L^\infty\left(0,T;C^6_{\rm per}(\Omega)\right). \tag{A.1}$$

Theorem A.1. *Given initial data $\Phi(\cdot, t=0) \in C^6_{\rm per}(\Omega)$, suppose the exact solution for the variable-mobility Cahn Hilliard equation (2) is of regularity class $\mathcal{R}$. Then, provided Δt and h are sufficiently small, and under the linear refinement requirement $\hat{C}_1 h \le \Delta t \le \hat{C}_2 h$, we have*

$$\|\Phi^k - \phi^k\|_2 + \Big(\Delta t \sum_{j=1}^{k} (\|\nabla_h(\Phi^j - \phi^j)\|_2^2\Big)^{1/2} \le C(\Delta t + h^2), \tag{A.2}$$

for all positive integers k, such that $t_k = k\Delta t \le T$, where $C > 0$ is independent of Δt and h.

Proof. A careful application of Taylor expansion for Φ gives

$$\frac{\Phi^{k+1} - \Phi^k}{\Delta t} = \nabla_h \cdot \Big(\breve{\mathcal{M}}^k \nabla_h \Big((\Phi^{k+1})^3 - \Phi^k - \varepsilon^2 \Delta_h \Phi^{k+1}\Big)\Big) + \tau^{k+1}, \tag{A.3}$$

with the local truncation error $\|\tau^{k+1}\|_2 \le C(\Delta t + h^2)$. In turn, the numerical error function is introduced at a point-wise level:

$$\tilde{\phi}^m = \Phi^m - \phi^m, \quad \forall m \ge 0. \tag{A.4}$$

In turn, subtracting (A.3) from (15) leads to

$$\begin{aligned}\frac{\tilde{\phi}^{k+1}-\tilde{\phi}^{k}}{\Delta t} = \nabla_h \cdot \Big(& (\breve{\mathcal{M}}(\Phi^k)-\breve{\mathcal{M}}^k)\nabla_h \mathcal{V}^{k+1} \\ & + \breve{\mathcal{M}}^k \nabla_h (\mathcal{N}_1^{k+1} - \tilde{\phi}^k - \varepsilon^2 \Delta_h \tilde{\phi}^{k+1}) \Big) + \tau^{k+1},\end{aligned} \tag{A.5}$$

where

$$\mathcal{N}_1^{k+1} := (\Phi^{k+1})^3 - (\phi^{k+1})^3 = \mathcal{N}_2^{k+1}\tilde{\phi}^{k+1}, \tag{A.6}$$

$$\mathcal{N}_2^{k+1} := (\Phi^{k+1})^2 + \Phi^{k+1}\phi^{k+1} + (\phi^{k+1})^2, \tag{A.7}$$

$$\mathcal{V}^{k+1} := (\Phi^{k+1})^3 - \Phi^k - \varepsilon^2 \Delta_h \Phi^{k+1}. \tag{A.8}$$

The exact solution Φ has the following bounds:

$$\|\Phi\|_{L^\infty(0,T*;W_h^{4,\infty})} \le C_5, \quad \|\Phi^m\|_6 \le C_5, \quad \forall m \ge 0. \tag{A.9}$$

Since $\mathcal{V}^{m+1}$ only depends on the exact solution, we assume a discrete $W^{1,\infty}$ bound:

$$\|\mathcal{V}^{m+1}\|_\infty + \|\nabla_h \mathcal{V}^{m+1}\|_\infty \le C_6, \quad \forall\, m \ge 0. \tag{A.10}$$

Since the numerical scheme (15) is unconditionally energy stable, we have

$$E_h(\phi^m) \le E_h(\phi^{m-1}) \le \cdots \le E_h(\phi^0) \le C_0, \tag{A.11}$$

so that

$$\|\phi^m\|_{H_h^1} \le \tilde{C}_0 := C\epsilon^{-1}(C_0 + C_\Omega). \tag{A.12}$$

Consequently, with an application of 3-D Sobolev inequality (C.1), we conclude that

$$\|\phi^m\|_6 \le C\|\phi^m\|_{H_h^1} \le \tilde{C}_1 := C\tilde{C}_0, \quad \forall m \ge 0. \tag{A.13}$$

In addition, we make an a-priori assumption for the numerical error function at the previous time step:

$$\|\nabla_h \tilde{\phi}^k\|_4 \le 1, \tag{A.14}$$

and this assumption will be recovered by the convergence estimate at the next time step. As a result, the $W_h^{1,4}$ bound of the numerical solution at t^k becomes available:

$$\|\nabla_h \phi^k\|_4 = \|\nabla_h(\Phi^k - \tilde{\phi}^k)\|_4 \le \|\nabla_h \Phi^k\|_4 + \|\nabla_h \tilde{\phi}^k\|_4 \le C_5 + 1. \tag{A.15}$$

Taking an inner product with (A.5) by $2\tilde{\phi}^{k+1}$ leads to

$$\begin{aligned}& \frac{1}{\Delta t}\Big(\|\tilde{\phi}^{k+1}\|_2^2 - \|\tilde{\phi}^k\|_2^2 + \|\tilde{\phi}^{k+1} - \tilde{\phi}^k\|_2^2 \Big) \\ & + 2\langle \nabla_h \tilde{\phi}^{k+1}, \breve{\mathcal{M}}^k \nabla_h (\mathcal{N}_1^{k+1} - \varepsilon^2 \Delta_h \tilde{\phi}^{k+1}) \rangle \\ =& 2\langle \nabla_h \tilde{\phi}^{k+1}, \breve{\mathcal{M}}^k \nabla_h \tilde{\phi}^k - (\breve{\mathcal{M}}(\Phi^k) - \breve{\mathcal{M}}^k)\nabla_h \mathcal{V}^{k+1} \rangle + 2\langle \tau^{k+1}, \tilde{\phi}^{k+1} \rangle,\end{aligned} \tag{A.16}$$

in which the summation by parts formulas have been applied.

For the right hand side terms, the following estimates are available:

$$2\langle \nabla_h \tilde{\phi}^{k+1}, \breve{\mathcal{M}}^k \nabla_h \tilde{\phi}^k \rangle \le 2\|\mathcal{M}(\phi^k)\|_\infty \cdot \|\nabla_h \tilde{\phi}^{k+1}\|_2 \cdot \|\nabla_h \tilde{\phi}^k\|_2$$

$$\le 2\mathcal{M}_1 \|\nabla_h \tilde{\phi}^{k+1}\|_2 \cdot \|\nabla_h \tilde{\phi}^k\|_2 \le \mathcal{M}_1 (\|\nabla_h \tilde{\phi}^{k+1}\|_2^2 + \|\nabla_h \tilde{\phi}^k\|_2^2), \tag{A.17}$$

$$|\mathcal{M}(\Phi^k) - \breve{\mathcal{M}}^k| = |\mathcal{M}'(\xi^{(k)})(\Phi^k - \phi^k)| = |\mathcal{M}'(\xi^{(k)})\tilde{\phi}^k| \le M|\tilde{\phi}^k|, \tag{A.18}$$

$$-2\langle \nabla_h \tilde{\phi}^{k+1}, (\breve{\mathcal{M}}(\Phi^k) - \breve{\mathcal{M}}^k)\nabla_h \mathcal{V}^{k+1} \rangle$$

$$\le 2\|\nabla_h \tilde{\phi}^{k+1}\|_2 \cdot \|\mathcal{M}(\Phi^k) - \breve{\mathcal{M}}^k\|_2 \cdot \|\nabla_h \mathcal{V}^{k+1}\|_\infty$$

$$\le 2C_5 \|\nabla_h \tilde{\phi}^{k+1}\|_2 \cdot M\|\tilde{\phi}^k\|_2 = 2C_5 M \|\nabla_h \tilde{\phi}^{k+1}\|_2 \cdot \|\tilde{\phi}^k\|_2$$

$$\le C_5 M (\|\nabla_h \tilde{\phi}^{k+1}\|_2^2 + \|\tilde{\phi}^k\|_2^2), \tag{A.19}$$

$$2\langle \tau^{k+1}, \tilde{\phi}^{k+1} \rangle \le \|\tau^{k+1}\|_2^2 + \|\tilde{\phi}^{k+1}\|_2^2, \tag{A.20}$$

in which $\xi^{(k)}$ is between ϕ^k and Φ^k. Notice that the uniform bounds for the mobility function, $\mathcal{M}_0 \le \mathcal{M}(\phi) \le \mathcal{M}_1$, as well as its derivative bound, $|\mathcal{M}'(\phi)| \le M$, and the $W_h^{1,\infty}$ bound (A.10) for $\mathcal{V}^{k+1}$, have been used in the derivation.

For the nonlinear error term, we focus on the inner product in the x direction; the corresponding analysis in the y and z directions could be similarly carried out. Over any fixed mesh cell, from (i, j, k) to $(i + 1, j, k)$, the following identities are valid:

$$D_x(fg) = (A_x f) \cdot (D_x g) + (A_x g) \cdot (D_x f), \ (A_x f)_{i+1/2,j,k} = \frac{1}{2}(f_{i,j,k} + f_{i+1,j,k}), \tag{A.21}$$

$$D_x \mathcal{N}_1^{k+1} = D_x(\mathcal{N}_2^{k+1} \tilde{\phi}^{k+1}) = (A_x \mathcal{N}_2^{k+1}) \cdot (D_x \tilde{\phi}^{k+1}) + (D_x \mathcal{N}_2^{k+1}) \cdot (A_x \tilde{\phi}^{k+1}). \tag{A.22}$$

For the first decomposition term in (A.22), we see that the nonlinear coefficient is non-negative at a point-wise level, i.e., $\mathcal{N}_2^{k+1} \ge 0$, so that

$$2\langle D_x \tilde{\phi}^{k+1}, \breve{\mathcal{M}}^k (A_x \mathcal{N}_2^{k+1}) \cdot (D_x \tilde{\phi}^{k+1}) \rangle \ge 0, \tag{A.23}$$

in which the fact that $\mathcal{M}(\phi^k) \ge \mathcal{M}_0$ has also been used. For the second decomposition term in (A.22), we look at the part of $D_x((\phi^{k+1})^2)$. A further application of the identity (A.21) implies that

$$D_x((\phi^{k+1})^2) = 2(A_x \phi^{k+1}) \cdot (D_x \phi^{k+1}), \quad \text{so that}$$

$$2\langle D_x \tilde{\phi}^{k+1}, \breve{\mathcal{M}}^k (D_x((\phi^{k+1})^2)) \cdot (A_x \tilde{\phi}^{k+1}) \rangle$$

$$= 4\langle D_x \tilde{\phi}^{k+1}, \breve{\mathcal{M}}^k (A_x \phi^{k+1}) \cdot (D_x \phi^{k+1}) \cdot (A_x \tilde{\phi}^{k+1}) \rangle \tag{A.24}$$

$$\le 4\|D_x \tilde{\phi}^{k+1}\|_6 \cdot \|\breve{\mathcal{M}}^k\|_\infty \cdot \|\phi^{k+1}\|_6 \cdot \|D_x \phi^{k+1}\|_2 \cdot \|\tilde{\phi}^{k+1}\|_6$$

$$\le C\|\Delta_h \tilde{\phi}^{k+1}\|_2 \cdot \mathcal{M}_1 \cdot \tilde{C}_0 \cdot \tilde{C}_1 \cdot \|\tilde{\phi}^{k+1}\|_{H_h^1} \le \tilde{C}_2 \|\Delta_h \tilde{\phi}^{k+1}\|_2 \cdot \|\tilde{\phi}^{k+1}\|_{H_h^1},$$

with $\tilde{C}_2 = C\tilde{C}_0 \tilde{C}_1 \mathcal{M}_1$, in which the discrete Sobolev inequalities (C.1), the discrete H^1 and L^6 bounds for the numerical solution, given by (A.12), (A.13), have been applied in the derivation. Similar estimates could be derived for two other expansion terms of $\mathcal{N}_2^{k+1}$; the results are stated below, while the technical details are skipped for the sake of brevity:

$$2\langle D_x \tilde{\phi}^{k+1}, \breve{\mathcal{M}}^k (D_x((\Phi^{k+1})^2)) \cdot (A_x \tilde{\phi}^{k+1}) \rangle \le \tilde{C}_3 \|\Delta_h \tilde{\phi}^{k+1}\|_2 \cdot \|\tilde{\phi}^{k+1}\|_{H_h^1},$$

$$2\langle D_x \tilde{\phi}^{k+1}, \breve{\mathcal{M}}^k (D_x(\Phi^{k+1}\phi^{k+1})) \cdot (A_x \tilde{\phi}^{k+1}) \rangle \le \tilde{C}_3 \|\Delta_h \tilde{\phi}^{k+1}\|_2 \cdot \|\tilde{\phi}^{k+1}\|_{H_h^1}, \tag{A.25}$$

with $\tilde{C}_3 = C(\tilde{C}_0\tilde{C}_1 + (C_5)^2)\mathcal{M}_1$. Subsequently, a combination of (A.23)-(A.25) leads to

$$2\langle D_x\tilde{\phi}^{k+1}, \breve{\mathcal{M}}^k D_x\mathcal{N}_1^{k+1}\rangle \le 3\tilde{C}_3\|\Delta_h\tilde{\phi}^{k+1}\|_2 \cdot \|\tilde{\phi}^{k+1}\|_{H_h^1}. \tag{A.26}$$

The estimates in the y and z directions are similar; the details are skipped for the sake of brevity:

$$\begin{aligned} &2\langle D_y\tilde{\phi}^{k+1}, \breve{\mathcal{M}}^k D_y\mathcal{N}_1^{k+1}\rangle \le 3\tilde{C}_3\|\Delta_h\tilde{\phi}^{k+1}\|_2 \cdot \|\tilde{\phi}^{k+1}\|_{H_h^1}, \\ &2\langle D_z\tilde{\phi}^{k+1}, \breve{\mathcal{M}}^k D_z\mathcal{N}_1^{k+1}\rangle \le 3\tilde{C}_3\|\Delta_h\tilde{\phi}^{k+1}\|_2 \cdot \|\tilde{\phi}^{k+1}\|_{H_h^1}. \end{aligned} \tag{A.27}$$

Then we obtain

(A.28)
$$\begin{aligned} 2\langle \nabla_h\tilde{\phi}^{k+1}, \breve{\mathcal{M}}^k\nabla_h\mathcal{N}_1^{k+1}\rangle \le& 9\tilde{C}_3\|\Delta_h\tilde{\phi}^{k+1}\|_2 \cdot \|\tilde{\phi}^{k+1}\|_{H_h^1} \\ \le& \frac{1}{2}\mathcal{M}_0\varepsilon^2\|\Delta_h\tilde{\phi}^{k+1}\|_2^2 + \frac{81}{2}\tilde{C}_3^2\mathcal{M}_0^{-1}\varepsilon^{-2}(\|\tilde{\phi}^{k+1}\|_2^2 + \|\nabla_h\tilde{\phi}^{k+1}\|_2^2). \end{aligned}$$

For the nonlinear error estimate associated with the surface diffusion part, the technical lemma in Appendix B is required. Finally, a substitution of (A.17)-(A.20), (A.28) and (B.1) into (A.16) results in

$$\begin{aligned} &\frac{1}{\Delta t}\Big(\|\tilde{\phi}^{k+1}\|_2^2 - \|\tilde{\phi}^k\|_2^2\Big) + \frac{1}{2}\mathcal{M}_0\varepsilon^2\|\Delta_h\tilde{\phi}^{k+1}\|_2^2 \\ \le& \tilde{C}_5(\|\nabla_h\tilde{\phi}^{k+1}\|_2^2 + \|\nabla_h\tilde{\phi}^k\|_2^2) + \tilde{C}_6(\|\tilde{\phi}^{k+1}\|_2^2 + \|\tilde{\phi}^k\|_2^2) + \|\tau^{k+1}\|_2^2. \end{aligned} \tag{A.29}$$

with $\tilde{C}_5 = \mathcal{M}_1 + C_5M + 81\tilde{C}_3^2\mathcal{M}_0^{-1}\varepsilon^{-2} + 2\varepsilon^2M^{(1)}$, $\tilde{C}_6 = C_5M + 81\tilde{C}_3^2\mathcal{M}_0^{-1}\varepsilon^{-2} + 1$, Meanwhile, an application of Cauchy inequality implies that

$$\begin{aligned} \tilde{C}_5\|\nabla_h\tilde{\phi}^m\|_2^2 =& -\tilde{C}_5\langle\tilde{\phi}^m, \Delta_h\tilde{\phi}^m\rangle \le \tilde{C}_5\|\tilde{\phi}^m\|_2 \cdot \|\Delta_h\tilde{\phi}^m\|_2 \\ \le& 2\tilde{C}_5^2\varepsilon^{-2}\|\tilde{\phi}^m\|_2^2 + \frac{1}{8}\mathcal{M}_0\varepsilon^2\|\Delta_h\tilde{\phi}^m\|_2^2, \quad m = k, k+1. \end{aligned} \tag{A.30}$$

A substitution of (A.30) into (A.29) results in

$$\begin{aligned} &\frac{1}{\Delta t}\Big(\|\tilde{\phi}^{k+1}\|_2^2 - \|\tilde{\phi}^k\|_2^2\Big) + \frac{1}{4}\mathcal{M}_0\varepsilon^2\|\Delta_h\tilde{\phi}^{k+1}\|_2^2 \\ \le& (\tilde{C}_6 + 2\tilde{C}_5^2\varepsilon^{-2})(\|\tilde{\phi}^{k+1}\|_2^2 + \|\tilde{\phi}^k\|_2^2) + \|\tau^{k+1}\|_2^2. \end{aligned} \tag{A.31}$$

An application of discrete Gronwall inequality implies that

$$\|\tilde{\phi}^{k+1}\|_2^2 + \frac{1}{4}\mathcal{M}_0\varepsilon^2\Delta t\sum_{\ell=1}^{k+1}\|\Delta_h\tilde{\phi}^\ell\|_2^2 \le C(\Delta t^2 + h^4), \tag{A.32}$$

so that an optimal rate convergence estimate has been established.

Recovery of the a-priori assumption (A.14)

With the optimal rate error estimate (A.32) at hand, we are able to obtain the following error bounds at time step t^{k+1}:

$$\|\tilde{\phi}^{k+1}\|_2 \le C(\Delta t + h^2), \quad \|\Delta_h\tilde{\phi}^{k+1}\|_2 \le \frac{C(\Delta t + h^2)}{\Delta t^{\frac{1}{2}}} \le C(\Delta t^{\frac{1}{2}} + h^{\frac{3}{2}}), \tag{A.33}$$

in which the linear refinement constraint $\hat{C}_1 h \le \Delta t \le \hat{C}_2 h$ has been applied. In turn, an application of the discrete Sobolev inequality (C.1) implies that

$$\|\nabla_h\tilde{\phi}^{k+1}\|_4 \le \|\Delta_h\tilde{\phi}^{k+1}\|_2 \le C(\Delta t^{\frac{1}{2}} + h^{\frac{3}{2}}) \le 1, \tag{A.34}$$

provided that Δt and h are sufficiently small. Therefore, the a-priori assumption (A.14) is valid at the next time step t^{k+1}, so that an induction analysis could be applied. This finishes the convergence analysis.

□

Appendix B. A technical lemma

The following technical lemma is needed in the proof of the convergence of the numerical scheme. The notation and the assumptions are the same.

Lemma B.1. *Under the point-wise bounds, $\mathcal{M}_0 \le \breve{\mathcal{M}}^k \le \mathcal{M}_1$, $|\mathcal{M}'(\phi)| \le M$, and the a-priori bound* (A.15) *for the numerical solution at the previous time step, we have*

$$\begin{aligned} &-\langle \nabla_h \tilde{\phi}^{m+1}, \breve{\mathcal{M}}(\phi^m) \nabla_h \Delta_h \tilde{\phi}^{m+1} \rangle \\ \ge &\frac{1}{2} \mathcal{M}_0 \| \Delta_h \tilde{\phi}^{m+1} \|_2^2 - M^{(1)} \| \nabla_h \tilde{\phi}^{m+1} \|_2^2, \end{aligned} \tag{B.1}$$

where the constant $M^{(1)}$ only depends on $\mathcal{M}_0$, $\mathcal{M}_1$, C_5, $\tilde{C}_1$ and M.

Proof. An application of summation by parts implies that

$$-\langle \nabla_h \tilde{\phi}^{m+1}, \breve{\mathcal{M}}(\phi^m) \nabla_h \Delta_h \tilde{\phi}^{m+1} \rangle = \langle \Delta_h \tilde{\phi}^{m+1}, \nabla_h \cdot (\breve{\mathcal{M}}(\phi^m) \nabla_h \tilde{\phi}^{m+1}) \rangle. \tag{B.2}$$

Meanwhile, at a fixed grid point (i, j, k), a detailed finite difference expansion reveals that

$$\begin{aligned} &\nabla_h \cdot (\breve{\mathcal{M}}(\phi^m) \nabla_h \tilde{\phi}^{m+1})_{i,j,k} \\ =&(\mathcal{M}\phi^m)_{i,j,k} \Delta_h \tilde{\phi}^{m+1}_{i,j,k} \\ &+ \frac{1}{2} (D_x (\mathcal{M}\phi^m)_{i+\frac{1}{2},j,k} D_x \tilde{\phi}^{m+1}_{i+\frac{1}{2},j,k} + D_x (\mathcal{M}\phi^m)_{i-\frac{1}{2},j,k} D_x \tilde{\phi}^{m+1}_{i-\frac{1}{2},j,k}) \\ &+ \frac{1}{2} (D_y (\mathcal{M}\phi^m)_{i,j+\frac{1}{2},k} D_y \tilde{\phi}^{m+1}_{i,j+\frac{1}{2},k} + D_y (\mathcal{M}\phi^m)_{i,j-\frac{1}{2},k} D_y \tilde{\phi}^{m+1}_{i,j-\frac{1}{2},k}) \\ &+ \frac{1}{2} (D_z (\mathcal{M}\phi^m)_{i,j,k+\frac{1}{2}} D_z \tilde{\phi}^{m+1}_{i,j,k+\frac{1}{2}} + D_z (\mathcal{M}\phi^m)_{i,j,k-\frac{1}{2}} D_z \tilde{\phi}^{m+1}_{i,j,k-\frac{1}{2}}). \end{aligned}$$

Subsequently, an application of discrete Hölder inequality leads to

$$\begin{aligned} &-\langle \nabla_h \tilde{\phi}^{m+1}, \breve{\mathcal{M}}(\phi^m) \nabla_h \Delta_h \tilde{\phi}^{m+1} \rangle \\ =&\langle \Delta_h \tilde{\phi}^{m+1}, \nabla_h \cdot (\breve{\mathcal{M}}(\phi^m) \nabla_h \tilde{\phi}^{m+1}) \rangle \\ \ge &\min(\mathcal{M}(\phi^m)) \cdot \| \Delta_h \tilde{\phi}^{m+1} \|_2^2 \\ &- \| \nabla_h (\mathcal{M}(\phi^m)) \|_4 \cdot \| \nabla_h \tilde{\phi}^{m+1} \|_4 \cdot \| \Delta_h \tilde{\phi}^{m+1} \|_2. \end{aligned} \tag{B.3}$$

Meanwhile, the following bound is available for $\| \nabla_h (\mathcal{M}\phi^m) \|_4$:

$$\begin{aligned} \| \nabla_h (\mathcal{M}(\phi^m)) \|_4 \le &(\| \mathcal{M}'(\xi) \|_\infty \cdot \| \phi^m \|_4 + \| \mathcal{M}(\phi) \|_\infty \cdot \| \nabla_h \phi^m \|_4) \\ \le &M \cdot C \tilde{C}_1 + \mathcal{M}_1 \| \nabla_h \phi^m \|_4 \\ \le &M \cdot C \tilde{C}_1 + \mathcal{M}_1 (C_5 + 1) := \tilde{C}_4, \end{aligned} \tag{B.4}$$

in which the a-priori estimates (A.13), (A.15) have been applied. Going back (B.3), we arrive at

$$
\begin{aligned}
&-\langle \nabla_h \tilde{\phi}^{m+1}, \breve{\mathcal{M}}(\phi^m)\nabla_h \Delta_h \tilde{\phi}^{m+1}\rangle \\
=&\langle \Delta_h \tilde{\phi}^{m+1}, \nabla_h \cdot (\breve{\mathcal{M}}(\phi^m)\nabla_h \tilde{\phi}^{m+1})\rangle \\
\geq&\mathcal{M}_0 \|\Delta_h \tilde{\phi}^{m+1}\|_2^2 - \tilde{C}_4 \|\nabla_h \tilde{\phi}^{m+1}\|_4 \cdot \|\Delta_h \tilde{\phi}^{m+1}\|_2 \\
\geq&\mathcal{M}_0 \|\Delta_h \tilde{\phi}^{m+1}\|_2^2 - C\tilde{C}_4 \|\nabla_h \tilde{\phi}^{m+1}\|_2^{\frac{1}{4}} \cdot \|\Delta_h \tilde{\phi}^{m+1}\|_2^{\frac{3}{4}} \cdot \|\Delta_h \tilde{\phi}^{m+1}\|_2 \\
\geq&\mathcal{M}_0 \|\Delta_h \tilde{\phi}^{m+1}\|_2^2 - C\tilde{C}_4 \|\nabla_h \tilde{\phi}^{m+1}\|_2^{\frac{1}{4}} \cdot \|\Delta_h \tilde{\phi}^{m+1}\|_2^{\frac{7}{4}} \\
\geq&\mathcal{M}_0 \|\Delta_h \tilde{\phi}^{m+1}\|_2^2 - \frac{1}{2}\mathcal{M}_0 \|\Delta_h \tilde{\phi}^{m+1}\|_2^2 - M^{(1)} \|\nabla_h \tilde{\phi}^{m+1}\|_2^2 \\
=&\frac{1}{2}\mathcal{M}_0 \|\Delta_h \tilde{\phi}^{m+1}\|_2^2 - M^{(1)} \|\nabla_h \tilde{\phi}^{m+1}\|_2^2,
\end{aligned}
\tag{B.5}
$$

in which the Sobolev inequality (C.2) has been applied in the second step, and the Young's inequality has been applied in the last step. Moreover, $M^{(1)}$ only depends on $\mathcal{M}_0$ and $\tilde{C}_4$, henceforth on $\tilde{C}_1$, C_5, $\mathcal{M}_1$ and M. This finishes the proof of Lemma B.1. □

Appendix C. Some discrete Sobolev inequalities

The following inequalities were used in the proof of convergence of the numerical scheme.

Lemma C.1. *For any 3-D periodic grid function f (over cell centered mesh points), we have*

$$
\|f\|_6 \leq C\|f\|_{H_h^1}, \quad \|\nabla_h f\|_6 \leq C\|\Delta_h f\|_2, \tag{C.1}
$$

$$
\|\nabla_h f\|_4 \leq C\|\nabla_h f\|_2^{\frac{1}{4}} \cdot \|\Delta_h f\|_2^{\frac{3}{4}}. \tag{C.2}
$$

Proof. Due to the periodic boundary conditions for f and its cell-centered representation, it has a corresponding discrete Fourier transformation:

$$
f_{i,j,k} = \sum_{\ell,m,n=-K}^{K} \hat{f}^N_{\ell,m,n} \mathrm{e}^{2\pi i(\ell x_{i+1/2} + m y_{j+1/2} + n z_{k+1/2})}, \tag{C.3}
$$

with $\hat{f}^N_{\ell,m,n}$ the discrete Fourier coefficients. And also, its extension to a continuous function is given by

$$
f_{\mathbf{F}}(x,y) = \sum_{\ell,m,n=-K}^{K} \hat{f}^N_{\ell,m,n} \mathrm{e}^{2\pi i(\ell x + m y + n z)}. \tag{C.4}
$$

Parseval's identity (at both the discrete and continuous levels) implies that

$$
\sum_{i,j,k=0}^{N-1} |f_{i,j}|^2 = N^3 \sum_{\ell,m,n=-K}^{K} |\hat{f}^N_{\ell,m,n}|^2, \quad \|f_{\mathbf{F}}\|^2 = \sum_{\ell,m,n=-K}^{K} |\hat{f}^N_{\ell,m,n}|^2. \tag{C.5}
$$

Based on the fact that $hN = L$, this in turn results in

$$
\|f\|_2^2 = \|f_{\mathbf{F}}\|^2 = \sum_{\ell,m=-K}^{K} |\hat{f}^N_{\ell,m,n}|^2. \tag{C.6}
$$

For the comparison between $f = D_x f$ and $\partial_x f_{\mathbf{F}}$, we look at the following Fourier expansions:

$$\begin{aligned} D_x f_{i+1/2,j,k} &= \frac{f_{i+1,j,k} - f_{i,j,k}}{2h} \\ &= \sum_{\ell,m,n=-K}^{K} \mu_\ell \hat{f}^N_{\ell,m,n} \mathrm{e}^{2\pi i(\ell x_{i+1} + m y_{j+1/2} + z_{k+1/2})}, \qquad \text{(C.7)} \\ \partial_x f_{\mathbf{F}}(x,y,z) &= \sum_{\ell,m,n=-K}^{K} \nu_\ell \hat{f}^N_{\ell,m,n} \mathrm{e}^{2\pi i(\ell x + m y + n z)}, \qquad \text{(C.8)} \end{aligned}$$

with

$$\mu_\ell = -\frac{2i\sin(\ell\pi h)}{h}, \quad \nu_\ell = -2\ell\pi i. \tag{C.9}$$

A comparison of Fourier eigenvalues between $|\mu_\ell|$ and $|\nu_\ell|$ shows that

$$\frac{2}{\pi}|\nu_\ell| \le |\mu_\ell| \le |\nu_\ell|, \quad \text{for} \quad -\mathrm{K} \le \ell \le \mathrm{K}, \tag{C.10}$$

which in turn leads to

$$\frac{2}{\pi}\|\partial_x f_{\mathbf{F}}\| \le \|D_x f\|_2 \le \|\partial_x f_{\mathbf{F}}\|. \tag{C.11}$$

A similar estimate could also be derived:

$$\frac{2}{\pi}\|\partial_y f_{\mathbf{F}}\| \le \|D_y f\|_2 \le \|\partial_y f_{\mathbf{F}}\|, \ \ \frac{2}{\pi}\|\partial_z f_{\mathbf{F}}\| \le \|D_z f\|_2 \le \|\partial_z f_{\mathbf{F}}\|. \tag{C.12}$$

A combination of (C.6), (C.11) and (C.12) yields

$$\frac{2}{\pi}\|f_{\mathbf{F}}\|_{H^1} \le \|f\|_{H^1_h} \le \|\boldsymbol{f}_{\mathbf{F}}\|_{H^1}. \tag{C.13}$$

Meanwhile, the following estimate has been established in recent works [8, 19]: *For a 3-D periodoic grid function f, we have*

$$\|f\|_p \le \sqrt{\frac{p}{2}}\|f_{\mathbf{F}}\|_{L^p}, \quad \text{with } p = 4, 6. \tag{C.14}$$

As a result, by taking $p = 6$, we obtain the discrete Sobolev inequality

$$\|f\|_6 \le \sqrt{3}\|f_{\mathbf{F}}\|_{L^6} \le C\|f_{\mathbf{F}}\|_{H^1} \le C\|f\|_{H^1_h}. \tag{C.15}$$

in which the Sobolev embedding (for continuous functions) has been applied at the second step, while the estimate (C.13) has been recalled in the last step.

The second inequality in (C.1) could be proved in a similar manner.

The inequality (C.2) is based on the following estimates

$$\|\nabla_h f\|_4 \le \sqrt{2}\|\nabla f_{\mathbf{F}}\|_{L^4}, \quad \text{(similarly)}, \tag{C.16}$$

$$\|\nabla_h f\|_2 \le \|\nabla f_{\mathbf{F}}\|, \quad \|\Delta_h f\|_2 \le \|\Delta f_{\mathbf{F}}\|, \tag{C.17}$$

$$\|\nabla f_{\mathbf{F}}\|_{L^4} \le C\|\nabla f_{\mathbf{F}}\|^{\frac{1}{4}} \cdot \|\Delta f_{\mathbf{F}}\|^{\frac{3}{4}}. \tag{C.18}$$

This finishes the proof of Lemma C.1. □

References

[1] S. M. Allen and J. W. Cahn. A microscopic theory for antiphase boundary motion and its application to antiphase domain coarsening. Acta. Metall., 27:1085, 1979.

[2] A. Baskaran, Z. Hu, J. Lowengrub, C. Wang, S.M. Wise, and P. Zhou. Energy stable and effi- cient finite-difference nonlinear multigrid schemes for the modified phase field crystal equation. J. Comput. Phys., 250:270-292, 2013.

[3] A. Baskaran, J. Lowengrub, C. Wang, and S.M. Wise. Convergence analysis of a second order convex splitting scheme for the modified phase field crystal equation. SIAM J. Numer. Anal., 51:2851-2873, 2013.

[4] J.W. Cahn and J.E. Hilliard. Free energy of a nonuniform system. i. interfacial free energy. J. Chem. Phys., 28:258-267, 1958.

[5] W. Chen, S. Conde, C. Wang, X. Wang, and S.M. Wise. A linear energy stable scheme for a thin film model without slope selection. J. Sci. Comput., 52:546-562, 2012.

[6] W. Chen, W. Feng, Y. Liu, C. Wang, and S.M. Wise. A second order energy stable scheme for the Cahn-Hilliard-Hele-Shaw equation. Discrete Contin. Dyn. Syst. Ser. B, 24:149-182, 2019.

[7] W. Chen, Y. Liu, C. Wang, and S.M. Wise. An optimal-rate convergence analysis of a fully discrete finite difference scheme for Cahn-Hilliard-Hele-Shaw equation. Math. Comp., 85:2231-2257, 2016.

[8] W. Chen, C. Wang, S. Wang, X. Wang, and S.M. Wise. Energy stable numerical schemes for ternary Cahn-Hilliard system. J. Sci. Comput., 84:27, 2020.

[9] W. Chen, C. Wang, X. Wang, and S.M. Wise. A linear iteration algorithm for energy stable second order scheme for a thin film model without slope selection. J. Sci. Comput., 59:574-601, 2014.

[10] K. Cheng, W. Feng, C. Wang, and S.M. Wise. An energy stable fourth order finite difference scheme for the Cahn-Hilliard equation. J. Comput. Appl. Math., 362:574-595, 2019.

[11] K. Cheng, C. Wang, and S.M. Wise. An energy stable Fourier pseudo-spectral numerical scheme for the square phase field crystal equation. Commun. Comput. Phys., 26:1335-1364, 2019.

[12] K. Cheng, C. Wang, S.M. Wise, and X. Yue. A second-order, weakly energy-stable pseudo-spectral scheme for the Cahn-Hilliard equation and its solution by the homogeneous linear iteration method. J. Sci. Comput., 69:1083-1114, 2016.

[13] A. Diegel, X. Feng, and S.M. Wise. Convergence analysis of an unconditionally stable method for a Cahn-Hilliard-Stokes system of equations. SIAM J. Numer. Anal., 53:127-152, 2015.

[14] A. Diegel, C. Wang, X. Wang, and S.M. Wise. Convergence analysis and error estimates for a second order accurate finite element method for the Cahn-Hilliard-Navier-Stokes system. Numer. Math., 137:495-534, 2017.

[15] A. Diegel, C. Wang, and S.M. Wise. Stability and convergence of a second order mixed finite element method for the Cahn-Hilliard equation. IMA J. Numer. Anal., 36:1867-1897, 2016.

[16] D.J. Eyre. Unconditionally gradient stable time marching the Cahn-Hilliard equation. MRS. Symp. Proc., 529:39, 1998.

[17] W. Feng, Z. Guan, J.S. Lowengrub, C. Wang, S.M. Wise, and Y. Chen. A uniquely solvable, energy stable numerical scheme for the functionalized Cahn-Hilliard equation and its convergence analysis. J. Sci. Comput., 76(3):1938-1967, 2018.

[18] W. Feng, A.J. Salgado, C. Wang, and S.M. Wise. Preconditioned steepest descent methods for some nonlinear elliptic equations involving p-Laplacian terms. J. Comput. Phys., 334:45-67, 2017.

[19] W. Feng, C. Wang, S.M. Wise, and Z. Zhang. A second-order energy stable Backward Differentiation Formula method for the epitaxial thin film equation with slope selection. Numer. Methods Partial Differ. Equ., 34:1975-2007, 2018.

[20] X. Feng and S.M. Wise. Analysis of a fully discrete finite element approximation of a Darcy-Cahn-Hilliard diffuse interface model for the Hele-Shaw flow. SIAM J. Numer. Anal., 50:1320-1343, 2012.

[21] Z. Guan, J.S. Lowengrub, and C. Wang. Convergence analysis for second order accurate schemes for the periodic nonlocal Allen-Cahn and Cahn-Hilliard equations. Math. Methods Appl. Sci., 40:6836-6863, 2017.

[22] Z. Guan, J.S. Lowengrub, C. Wang, and S.M. Wise. Second-order convex splitting schemes for nonlocal Cahn-Hilliard and Allen-Cahn equations. J. Comput. Phys., 277:48-71, 2014.

[23] Z. Guan, C. Wang, and S.M. Wise. A convergent convex splitting scheme for the periodic nonlocal Cahn-Hilliard equation. Numer. Math., 128:377-406, 2014.

[24] J. Guo, C. Wang, S.M. Wise, and X. Yue. An H^2 convergence of a second-order convex-splitting, finite difference scheme for the three-dimensional Cahn-Hilliard equation. Commu. Math. Sci., 14:48-515, 2016.
[25] J. Guo, C. Wang, S.M. Wise, and X. Yue. An improved error analysis for a second-order numerical scheme for the Cahn-Hilliard equation. J. Comput. Appl. Math., 388:113300, 2021.
[26] D. Han and X. Wang. A second order in time, uniquely solvable, unconditionally stable numerical scheme for Cahn-Hilliard-Navier-Stokes equation. J. Comput. Phys., 290:139-156, 2015.
[27] Z. Hu, S. Wise, C. Wang, and J.S. Lowengrub. Stable and efficient finite-difference nonlinear multigrid schemes for the phase–ield crystal equation. J. Comput. Phys., 228:5323-5339, 2009.
[28] Y. Huang, R. Li, and W. Liu. Preconditioned descent algorithms for p-Laplacians. J. Sci. Comput., 32:343-371, 2007.
[29] R.V. Kohn and X. Yan. Upper bound on the coarsening rate for an epitaxial growth model. Comm. Pure Appl. Math., 56:1549-564, 2003.
[30] D. Li and Z. Qiao. On second order semi-implicit Fourier spectral methods for 2D Cahn-Hilliard equations. J. Sci. Comput., 70:301-341, 2017.
[31] D. Li and Z. Qiao. On the stabilization size of semi-implicit Fourier-spectral methods for 3D Cahn-Hilliard equations. Commun. Math. Sci., 15:1489-1506, 2017.
[32] D. Li, Z. Qiao, and T. Tang. Characterizing the stabilization size for semi-implicit Fourier-spectral method to phase field equations. SIAM J. Numer. Anal., 54:1653-1681, 2016.
[33] C. Liu, C. Wang, S.M. Wise, X. Yue, and S. Zhou. An iteration solver for the Poisson-Nernst-Planck system and its convergence analysis. J. Comput. Appl. Math., 406:114017, 2022.
[34] J. Shen, C. Wang, X. Wang, and S.M. Wise. Second-order convex splitting schemes for gradient flows with Ehrlich-Schwoebel type energy: Application to thin film epitaxy. SIAM J. Numer. Anal., 50:105-125, 2012.
[35] J. Shen and J. Xu. Convergence and error analysis for the scalar auxiliary variable (SAV) schemes to gradient flows. SIAM J. Numer. Anal., 56:2895-2912, 2018.
[36] J. Shen, J. Xu, and J. Yang. The scalar auxiliary variable (SAV) approach for gradient flows. J. Comput. Phys., 353:407-416, 2018.
[37] J. Shen, J. Xu, and J. Yang. A new class of efficient and robust energy stable schemes for gradient flows. SIAM Review, 61:474-506, 2019.
[38] C. Wang, X. Wang, and S.M. Wise. Unconditionally stable schemes for equations of thin film epitaxy. Discrete Contin. Dyn. Syst., 28:405-423, 2010.
[39] C. Wang and S.M. Wise. An energy stable and convergent finite-difference scheme for the modified phase field crystal equation. SIAM J. Numer. Anal., 49:945-969, 2011.
[40] L. Wang and H. Yu. On efficient second order stabilized semi-implicit schemes for the Cahn-Hilliard phase-field equation. J. Sci. Comput., 77:1185-1209, 2018.
[41] S.M. Wise. Unconditionally stable finite difference, nonlinear multigrid simulation of the Cahn-Hilliard-Hele-Shaw system of equations. J. Sci. Comput., 44:38-68, 2010.
[42] S.M. Wise, C. Wang, and J.S. Lowengrub. An energy stable and convergent finite-difference scheme for the phase field crystal equation. SIAM J. Numer. Anal., 47:2269-2288, 2009.
[43] Y. Yan, W. Chen, C. Wang, and S.M. Wise. A second-order energy stable BDF numerical scheme for the Cahn-Hilliard equation. Commun. Comput. Phys., 23:572-602, 2018.
[44] J. Zhang, C. Wang, S.M. Wise, and Z. Zhang. Structure-preserving, energy stable numerical schemes for a liquid thin film coarsening model. SIAM J. Sci. Comput., 43:A1248-A1272, 2021.

Department of Mathematics, The University of Massachusetts, North Dartmouth, MA 02747, USA
E-mail: xchen2@umassd.edu and cwang1@umassd.edu

Department of Mathematics, The University of Tennessee, Knoxville, TN 37996, USA
E-mail: swise1@utk.edu